NTNU
Norwegian University of
Science and Technology

Modeling and Simulation of a Super-redundant Marine Power Plant as a Hybrid Dynamical System

Erlend Kvam Gurvin

Marine Technology
Submission date: June 2017
Supervisor: Roger Skjetne, IMT

Norwegian University of Science and Technology
Department of Marine Technology

NTNU Trondheim
Norwegian University of Science and Technology
Department of Marine Technology

MSC THESIS DESCRIPTION SHEET

Name of the candidate: Gurvin, Erlend Kvam

Field of study: Marine control engineering

Thesis title (Norwegian): Modellering og simulering av eit superredundant maritimt kraftanlegg som eit hybrid dynamisk system

Thesis title (English): Modeling and simulation of a super-redundant marine power plant as a hybrid dynamical system

Background

During the last 20 years, maritime electric installations have increased in size and scope, ranging from only few systems and installations to become an industry standard. The Norwegian maritime industry is taking a leading role in the development of advanced technology improving safety and performance of offshore vessels. Increased demands for energy-efficient and low emission multifunctional vessels with high availability and reliability have motivated electrically powered vessels with improved power and energy management systems (PMS/EMS). In addition, a shift towards more complex electric energy production systems with hybrid power plants using energy sources such as diesel, LNG, fuel cells, and additional energy storage devices such as battery banks, super-capacitors, and flywheels.

There has also been an extensive development in the automotive industry towards more energy-efficient engines, with rapid and robust start/stop functionality, combined with battery packs to reduce emissions and fuel consumption. Based on this, a PhD study is conducted at NTNU on how a marine power plant can be driven by a large number of small engines, e.g. truck engines, as opposed to the traditional large marine engines. In addition, ESDs should supplement such a system to e.g. reduce engine transient behavior. This will next require a larger and more complicated load-sharing system and PMS functions for rapid start/stop of engines, including coordination between the battery management system (BMS) and the PMS.

In this project we will explore the methods of hybrid dynamical systems to efficiently model and simulate the start/stop functionality of the engines, connect/disconnect functionality of the gensets and ESDs, and the continuous dynamics of the devices during the relevant modes (states) of operation.

Work description

1) Perform a background and literature review to provide information and relevant references on:
   a) Hybrid marine power plants; power producers, electric storage devices, converters, breakers, etc. and their main properties and dynamic characteristics (models).
   b) PMS; main objectives and functions, especially the load-dependent start/stop functionality.
   c) Load-sharing techniques in marine power plants.
   d) Modeling of marine power plants.
   e) Modeling and simulation framework for hybrid dynamical systems.

   Write a list with abbreviations and definitions of terms, explaining relevant concepts related to the literature study and project assignment.

2) Perform modeling and simulation of a marine power plant (see work note “Load-dependent start and stop of gensets modeled as a hybrid dynamical system”. This should be able to model from 1 to 30 gensets, but use 4 as a case in the beginning. The model needs updates:
   a) Update the genset and bus model based on the MSS Marine Power Plant Simulator.
   b) The logic variable for start/stop engine should be included, using ‘c’ as variable for “connected” and ‘s’ as variable for “started”.
   c) Implement with a defined start sequence and a typical start/stop table.

d) There should be an electric part with representation of reactive power. That is, the equivalent circuit model of the bus that is used to calculate load-sharing should be included, as well as governors and AVRs based on droop load-sharing. We will limit the model to the main bus.
e) Include necessary synchronization function that ensures approximately that $\omega = \omega_{bus}$ and $V = V_{bus}$ before connect is allowed. This needs an "InSynch" signal that indicates if synchronization is achieved. Phase is automatically synchronized since load angle is zero when disconnected.
f) Include load-up ramp and deload ramp when connecting and disconnecting a genset.
g) Use the HDS theory as a convenient modeling framework.

3) Based on your studies and insight, discuss performance and limitations of small vs. large engines:
   a) Typical efficiencies.
   b) Typical fuel economy / fuel curves.
   c) Other properties, e.g. ability for rapid start/stop, response to dynamic load variations, etc.?

4) Dimension a marine power plant according to a typical power capacity:
   a) Define test cases with respect to loading condition, e.g. a deterministic case and a typical load profile for a vessel.
   b) Do a study where the power plant is dimensioned with its capacity divided on, from 4 big to 10 smaller equally sized gensets. For each configuration run your test cases and analyze the results. One KPI is the ratio between total produced power and total online capacity (power utilization). Another KPI is the total fuel consumption from the plant. Can you plot these KPIs?

5) Discuss:
   a) Pros and cons related to operation and maintenance of the plant configurations.
   b) Redundancy and resilience to failures in power plant.

Tentatively:

6) Consider the following extensions:
   a) Include a power/rpm/fuel lookup table, based on typical curves, as a fuel measurement output from each engine.
   b) Is there a possibility to get some curves/lookup tables on emissions?

Specifications

The scope of work may prove to be larger than initially anticipated. By the approval from the supervisor, described topics may be deleted or reduced in extent without consequences with regard to grading.

The candidate shall present personal contribution to the resolution of problems within the scope of work. Theories and conclusions should be based on mathematical derivations and logic reasoning identifying the various steps in the deduction.

The report shall be organized in a logical structure to give a clear exposition of background, results, assessments, and conclusions. The text should be brief and to the point, with a clear language. Rigorous mathematical deductions and illustrating figures are preferred over lengthy textual descriptions. The report shall have font size 11 pts. It shall be written in English (preferably US) and contain the following elements: Title page, abstract, acknowledgements, thesis specification, list of symbols and acronyms, table of contents, introduction with objective, background, and scope and delimitations, main body with problem formulations, derivations/developments and results, conclusions with recommendations for further work, references, and optional appendices. All figures, tables, and equations shall be numerated. The original contribution of the candidate and material taken from other sources shall be clearly identified. Work from other sources shall be properly acknowledged using quotations and a Harvard citation style (e.g. *natbib* Latex package). The work is expected to be conducted in an honest and ethical manner, without any sort of plagiarism and misconduct. Such practice is taken very seriously by the university and will have consequences. NTNU can use the results freely in research and teaching by proper referencing, unless otherwise agreed upon.

The thesis shall be submitted with a printed and electronic copy to the main supervisor, with the printed copy signed by the candidate. The final revised version of this thesis description must be included. The report must be submitted according to NTNU procedures. Computer code, pictures, videos, data series, and a PDF version of the report shall be included electronically with all submitted versions.

Start date: 15 January, 2017 **Due date:** As specified by the administration.

Supervisor: Roger Skjetne
Co-advisor(s): Laxminarayan Thorat, Michel Miyazaki, Torstein I. Bø, Nicolas Lefebvre

Trondheim,

_____

Roger Skjetne
Supervisor

Preface

This Master Thesis in marine power plant engineering at NTNU is part of the study program Marine Technology. A preliminary project to the thesis was done in the autumn semester of 2016, while the Master Thesis was written during the spring semester of 2017. I worked as an intern for Marintek during the summer of 2016 with hybrid marine power plants. The topic of marine electrical systems was interesting to me, and when Professor Roger Skjetne presented the project *Modeling and simulation of a super-redundant marine power plant as a hybrid dynamical system* I contacted Roger, and the thesis was decided.

Trondheim, 2017-06-07

Erlend Kvam Gurvin

Acknowledgment

I would like to thank my supervisor, Professor Roger Skjetne, for developing a structured thesis description and guiding me through the semester. I would also like to thank my Co-supervisors Laxminarayan Thorat, Torstein Ingebrigtsen Bø and Michel Miyazaki, for always being available and helpful.

A special thanks to my parents who have supported me through my five year education in Trondheim, this would not be possible without you.

E.K.G.

Summary and Conclusions

During the last years the maritime industry has experienced increased demands in energy efficient and low emission vessels with high reliability and availability. These demands have been a motivation for electrical powered vessels with smarter power management systems. A diesel electric marine propulsion system converts power produced by diesel engines to electric power, which is distributed to the on-board consumers. Diesel electric propulsion offers more flexibility as the power plant consists of multiple diesel engine and generator pairs, called gensets. Diesel electric propulsion is especially efficient during operations with varying power demand, such as dynamical positioning.

A super-redundant marine power plant consists of many small gensets, up to thirty, while a conventional diesel electric marine power plant consist of four larger gensets. Diesel engines are the most fuel-efficient while operating at about 80% of their rated power. By increasing the number of engines making up a marine power plant, the engines would run at their most fuel-efficient power for a larger portion of operations. However, smaller engines are generally less efficient than larger ones. The thesis considers if there are any benefits in using a super-redundant marine power plant.

A model describing both mechanical and electrical aspects of a marine power plant is developed based on hybrid dynamical system theory. This allows the modeling of both the continuous and discrete changes of states in the power plant. The model is designed with a load control strategy which connects and disconnects gensets to the electrical grid based on the power consumption and a start/stop table. The model is shown to successfully connect and disconnect gensets with the synchronization and ramping that is necessary to do so, and provide equal load sharing among the active gensets.

A case study shows how a conventional four-genset marine power plant configuration outperforms a ten-genset configuration at loads above half the total capacity, while at lower loads the difference is negligible. The start/stop table in the case study were not properly tuned for the gensets, resulting in the super-redundant power plant not operating at optimal loading conditions. Considering a properly tuned start/stop table, the ten-genset marine power plant could

potentially reduce fuel consumption with up to 4% compared to that of the case study, this would suggest that a super-redundant marine power plant is more efficient than conventional configurations, especially while operating below 50% of the power plants total power capacity.

There are potential savings in maintenance for vessels with super-redundant power plants that often visit the same port. Due to the gensets relatively small size, a faulty genset could be swapped with a functioning one at port, reducing costly maintenance and downtime at sea. Redundancy would be greatly improved by increasing the number of gensets, as a single fault would have a significantly smaller impact on the total power output of the power plant.

With potential savings on fuel consumption, emissions, maintenance, and an increased redundancy, a super-redundant marine power plant could become commercially viable and contribute to reduce emissions from maritime industry.

Samandrag og Konklusjon

I løpet av dei siste åra har det vorte auka krav til energieffektive skip og lågare utslepp, samt sett krav til høgare pålitelegheit og tilgjengelegheit enn før. Dette har motivert for elektrisk drivne skip med smartare kraftstyringssystem. Diesel-elektriske marine propulsjonssystem konverterar kraft frå dieselmotorar til elektrisk kraft, som vert distribuert til forbrukarar ombord. Diesel-elektrisk propulsjon tilbyr meir fleksibilitet, sidan kraftanlegget består av består av fleire dieselmotor og generator par, kalla generatorsett. Diesel-elektrisk propulsjon er spesielt effektiv under operasjonar med eit varierande kraftbehov, som til dømes ved dynamisk posisjonering.

Eit super-redundant marint kraftanlegg består av mange mindre generatorsett, opp til tretti, medan eit meir konvensjonelt diesel-elektrisk kraftanlegg består av fire store generatorsett. Dieselmotorar er mest drivstoffeffektive når dei arbeider på 80% av maks kraft. Ved å auke antalet motorar i kraftanlegget, så kan motorane styrast til å arbeide nærmare sin mest drivstoffeffektive last for ein større del av tida. På ei anna side så er mindre motorar generelt sett mindre effektive enn dei som er større. Denne avhandlinga ser på om det er nokon fordelar ved å nytte super-redundante marine kraftsystem.

Ein modell er utvikla som beskriv mekaniske og elektriske aspekt ved eit marint kraftanlegg, basert på *hybrid dynamisk system*-teori. Dette gir moglegheta til å modellere både kontinuerlege og diskrete tilstandsendringar i kraftanlegget. Modellen er designa med ein last-kontrollstrategi som automatisk koplar av og på generatorsett basert på kraftforbruk og ein start/stopp-tabell. Modellen handterer nødvendig synkronisering samt å gradvis auke og minke lasta på generatorsett som koplast på og av. Modellen sikrar og ei lik lastfordeling på dei aktive generatorsetta.

Ein case er gjennomført der eit konvensjonelt marint kraftanlegg med fire store generatorsett er samanlikna med eit super-redundant kraftanlegg med ti mindre generatorsett. For laster over halve den totale kapasiteten til anlegget er fire-generatorsett konfigurasjonen mest effektiv, medan for mindre laster er forskjellar neglisjerbare. Start/stopp tabellen under simuleringane var ikkje skikkeleg justert for generatorsetta, som førte til at det super-redundante kraftanlegget ikkje opererte under optimale lastforhald. Dersom start/stopp tabellen var justert riktig, kunne drivstofforbruket blitt redusert med opp mot 4% samanlikna med resultatet frå simuleringa.

Dette gir at eit super-redundant marint kraftanlegg er meir drivstoffeffektiv enn konvensjonelle kraftanlegg for operasjonar under 50% av kraftanleggets totale kapasitet.

Det er potensielle besparingar i vedlikehald for skip med super-redundante kraftanlegg som ofte besøker same havn. Sidan generatorsetta er relativt små, er det enklare å bytte ut eit generatorsett som ikkje fungera med eit fungerande i havn, noko som redusera dyrt vedlikehald til sjøs. Redundans blir svært forbedra ved å auke antalet generatorsett, sidan eitt einskild motorhavari ville påverka den totale kapasiteten til kraftanlegget i mykje mindre grad.

Med potensielle besparingar i drivstofforbruk, utslepp, vedlikehald, og auka redundans, kan super-redundante marine kraftanlegg bli kommersielt levedyktige og bidra til å redusere utslepp fra maritim industri.

Contents

List of Figures

List of Tables

Glossary

Bus	An electrical utility which handles distribution of electrical power.
Genset	A diesel engine and a generator producing electrical power to the bus.
Bus load	The power demand on the bus.
Hybrid Power Plant	The combination of electrical producers with electrical storage devices in a power plant.
HDS	Hybrid Dynamical System, the combination of continuously and discretely changing states in a model.

List of Acronyms

PMS	**P**ower **M**anagement **S**ystem
EMS	**E**nergy **M**anagement **S**ystem
ESD	**E**nergy **S**torage **D**evice
IMO	**I**nternational **M**aritime **O**rganization
BAU	**B**usiness **A**s **U**sual
DP	**D**ynamical **P**ositioning
MCR	**M**aximum **C**ontinuous **R**ating
SFOC	**S**pecific **F**uel **O**il **C**onsumption
AVR	**A**utomatic **V**oltage **R**egulator
SOC	**S**tate **O**f **C**harge
DOD	**D**epth **O**f **D**ischarge
AC	**A**lternating **C**urrent
DC	**D**irect **C**urrent
HDS	**H**ybrid **D**ynamical **S**ystem
FOC	**F**uel **O**il **C**onsumption

Nomenclature

AVR symbols

ξ_{avr}	Integration bias
K_i	Integration gain
K_p	Proportional gain
T_{avr}	Low-pass filter time constant
V_{avr}	Unfiltered Field voltage
$V_{f,ref}$	Reference field voltage
V_f	Field voltage
V_{nl}	No load voltage

Bus symbols

δ_{bus}	Bus electric load angle
ω_{bus}	Bus electric frequency
E_t	Thevenin equivalent voltage
P_{bus}	Active load on bus
Q_{bus}	Reactive load on bus
S_{bus}	Load on bus
V_{bus}	Bus voltage
Z_t	Thevenin equivalent impedance

Engine symbols

ω	Angular frequency of shaft
τ_e	Electrical torque on shaft
τ_m	Mechanical torque on shaft
D	Linear damping coefficient
J	Shaft moment of inertia

Generator symbols

δ	Load angle of shaft
E	Induced line-to-neutral voltage
I	Generator current
p	Active power produced
q	Reactive power produced
s	Power produced by a generator
V_t	Terminal line-to-neutral voltage
Z	Generator impedance

Load control symbols

Ω	Boolean declaring if a genset is disconnecting from the bus
Ψ	Boolean declaring if a genset is connecting to the bus
τ_{HH}	Timer for hasty connection
τ_H	Timer for regular connection
τ_L	Timer counting up for a disconnect
c	Binary vector of connected generator sets
c_t	Time of connection
n	Number of generator sets connected to the bus

p_{avg} Average load on generator sets

p_{HH} Extra high power limit

p_H High power limit

p_L Lower power limit

Governor symbols

ω_{NL} No load frequency

ω_{ref} Reference shaft frequency

ξ Integration bias

K_d Derivative gain

K_i Integration gain

K_p Proportional gain

u Controlled torque input to shaft

Chapter 1

Introduction

1.1 Background

During the last years the maritime industry has experienced increased demands in energy efficient and low emission vessels with high reliability and availability. These demands have motivated for electrically powered vessels with smarter and more robust power and energy management systems(PMS/EMS). The industry is constantly innovating to increase efficiency and reduce emissions, with for instance hybrid power production. The term hybrid power system refers to power plants which combine power generation from engines with energy storage devices(ESD) such as batteries, super-capacitors and flywheels. Hybrid power systems enable possibilities for the PMS and EMS to be optimized for lower emissions and an over all reduced fuel consumption

Lately there has been a considerable development towards energy efficient engines in the automotive industry, with focus on rapid and robust start/stop functions combined with ESDs to reduce fuel consumption followed by reduced emissions. With the recent signing of the Paris agreement, further pressure is put on the maritime industry to reduce emissions, and one solution may be to follow the automotive industry in hybridization.

A PhD study conducted at NTNU on how a marine power plant can be driven by a larger number of smaller engines instead of the traditional large marine engines. A solution such as this may reduce fuel consumptions but will also require more comprehensive load-sharing

strategies and coordination of start/stop-systems for engines. With a larger number of smaller engines, marine power plants could be operating at ideal loading conditions for a larger periods than a conventional power plant with fewer and larger engines. This could potentially reduce fuel consumption and emissions.

1.1.1 Global emissions

Approximately 90 percent of world trade is carried at sea (IMO, 2012). During the years 2007 to 2012 it is estimated that international maritime transport is responsible for an annual average of 866 million tonnes of CO_2 which makes up 2.6 percent of global emissions in that six-year period (IMO, 2014). These numbers increase with the inclusion of fishing activity and domestic shipping to 1,015 million tonnes CO_2 and a total of 3.1 percent of global emissions. Even though shipping is undoubtedly the most efficient way of transport in terms of emitted CO_2 per tonne-km, the marine sector is striving for a reduction of emissions (IMO, 2009) (IMO, 2014).

The International Maritime Organization (IMO) have developed projections of shipping CO_2 emissions in the years 2012 to 2050 where different scenarios are presented. Their latest projections are presented in Figure 1.1. The Business-as-usual (BAU) projections indicate how the annual emissions will develop in the absence of any new regulations.

To stabilize global emissions of CO_2 at a level which results in a less than 2 °C rise in average global temperature by 2050, emissions from the maritime industry must be stabilized or reduced, or these projected values will account for 10-20% of all total permissible CO_2 emissions (Eleftherios K. Dedes, 2012). The internatiolan political goals are not compatible with the trends shown in Figure 1.1, and the maritime industry must look to reduce its carbon footprint.

CO_2 emissions are directly related to the fuel consumption of the vessels. To reduce overall emissions without reducing the capacity of the maritime industry, the fuel consumption of today's and future ships must be decreased. There are several factors influencing a vessels fuel

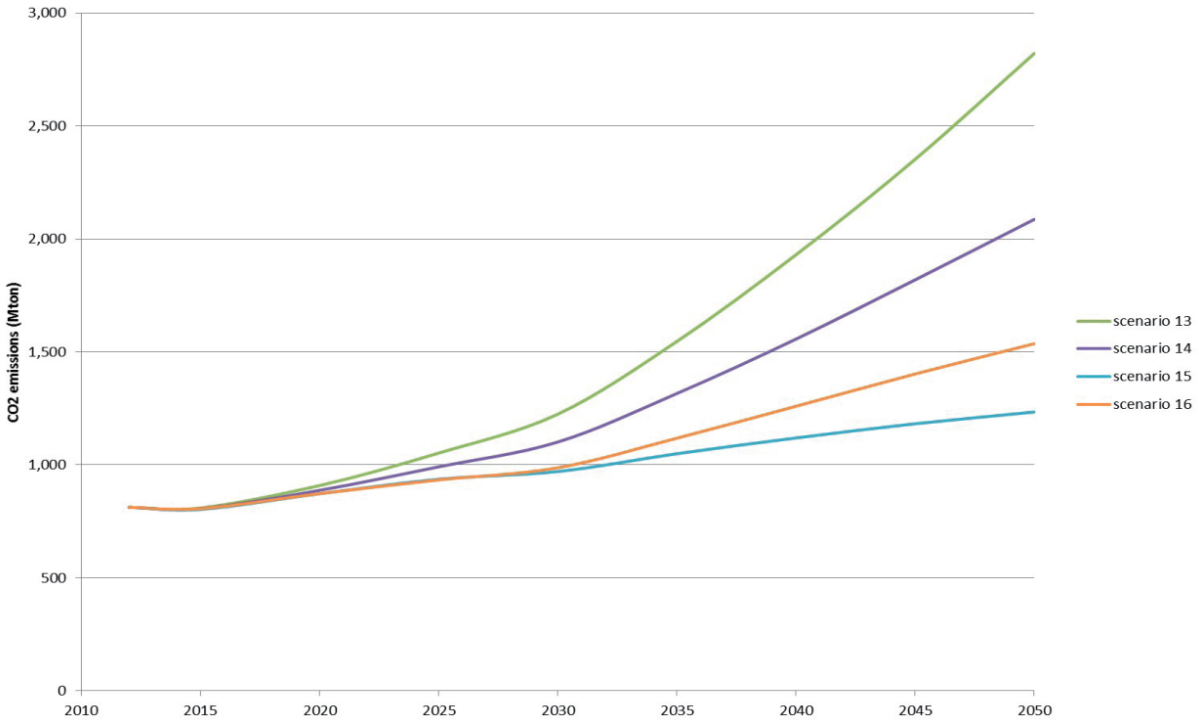

Figure 1.1: BAU projections of annual CO_2 emissions from international maritime transport (IMO, 2014).

consumption, such as the geometric design of the hull, the shape and size of the propellers and the efficiency of the machinery.

1.1.2 Diesel Electric Propulsion

Diesel Electric propulsion is widely used on vessels such as offshore supply vessels, ferries, cruise vessels and vessels with dynamical positioning (DP) systems. The power produced on a diesel electric vessel comes from the power plant, which consists of multiple pairs of diesel engines and electric generators; a diesel engine and a generator is called a generator set or genset. The power produced is distributed to the vessels consumers such as propulsion, hotel loads, equipment on deck and auxiliary systems (Ingebrigtsen Bø, 2016).

Diesel Electric propulsion offers more flexibility as the power plant can be easily reconfigured, and the optimal number of engines can be running to increase the overall efficiency and consequently reduce total emissions. An engine has an optimal working condition, which normally is around at 80 percent of maximum load, this is described in section 2.1. By using the amount of engines such that each engine is working as close the optimal loading condition will

increase the fuel efficiency of the overall system and reduce emissions.

1.2 Scope

The thesis looks into developing a hybrid dynamical system based of the MSS Marine Power Plant Simulator (Torstein I. Bø, 2015) and the Load-dependent start and stop of gensets modeled as a hybrid dynamical systems (Skjetne, 2016). The model should perform the necessary synchronization and load ramping before and after a genset is connected or disconnected from the bus, while ensuring there are always sufficient power available to supply the demanded load.

The power capacity of a marine power plant will be studied for a test case with load profile designed to show the functionality of the model. The capacity of the plant will be divided equally among a few large engines, and then among many smaller engines. Simulations are done with different number of engines making up the power plant to study the effect using super-redundant marine power plants potentially have on fuel consumption.

1.3 Limitations

The study is limited to a marine power plant using diesel engines as prime movers, and no energy storage devices such as batteries or super-capacitors.

The simulations are only lasting for 14 minutes, due to significant simulation times. This results in a load profile that does not accurately represent a typical load profile of a vessel.

The thesis only looks into fuel consumption of different power plant configurations, as CO_2 emissions is assumed to be proportional to fuel consumption. NO_x and SO_x emissions are not studied.

1.4 Structure of the Report

The rest of the report is organized as follows.

Chapter 2 gives an introduction to Hybrid Marine Power Plants, its components and their main properties.

Chapter 3 gives an introduction to Power and Energy Management Systems, load-dependent start/stop functionality and load-sharing teqniques in marine power plants.

Chapter 4 gives a framework for modeling and simulation of Hybrid Dynamical Systems.

Chapter 5 shows the Modeling of the Marine Power Plant as a Hybrid Dynamical Model.

Chapter 6 seek to Verify the Marine Power Plant Model.

Chapter 7 gives a short introduction to Efficiencies of Marine Diesel Engines.

Chapter 8 is a Case Study of a Marine Power Plant with a Varying Load.

Chapter 9 discuss Operation, Maintenance and Redundancy.

Chapter 10 present Conclusions and a Recommendation for Further Work.

Chapter 2

Hybrid Marine Power Plant

The hybrid marine power plant is a diesel electric propulsion system which uses prime movers for power generation and energy storage devices (ESDs), such as batteries, for temporary storage of energy as the name suggests. The power plant consists of multiple components for power production, storage, conversion and distribution.

2.1 Diesel Engine and Governor

The power source in an marine electric power plant is in most cases a diesel engine driving a generator. Direct mechanical propulsion utilizes low speed diesel engines while in modern diesel-electric propulsion systems, the prime movers are usually medium to high-speed diesel engines with lower weight and costs than the low speed engines (Ådnanes, 2003). With multiple engines the systems total availability increases as the system is more redundant and flexible for maintenance.

Diesel engines have different efficiencies at different Maximum Continuous Ratings (MCR). MCR is defined as the maximum power that the diesel engine is able to produce without overheating or being damaged. MCR is also known as rated power. Figure 2.1a show the specific fuel oil consumption (SFOC) of a single diesel engine for different loading percentages of the engines mean continuous rating (MCR), the SFOC is a measure of the engines efficiency in converting fuel to rotational energy. In optimal loading conditions a medium speed diesel engine

has a SFOC of less than 200g/KWh. Even though this may be regarded as an efficient engine, only 40 percent of the energy in the fuel is utilized, the rest disappears through exhaust or heat dissipation (Ådnanes, 2003).

For loading conditions below 50 percent MCR the SFOC rapidly increases, causing the efficiency of the engine to drop and an unnecessary amount of fuel is used. At this working condition the combustion is inefficient with high NOx and SOx content and with a high degree of soothing which increases the need for maintenance (Ådnanes, 2003). The goal of a diesel electric system is to use multiple smaller diesel engines to optimize the percentage loading by running the correct amount of engines at a given time, this can be achieved by starting and stopping generator sets depending on the demanded load to achieve an optimal loading condition on each generator set. The SFOC of multiple generator sets is shown in Figure 2.1b.

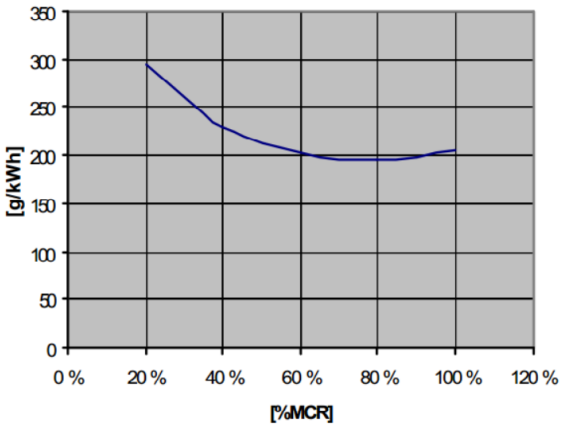

(a) Fuel consumption of a single engine.

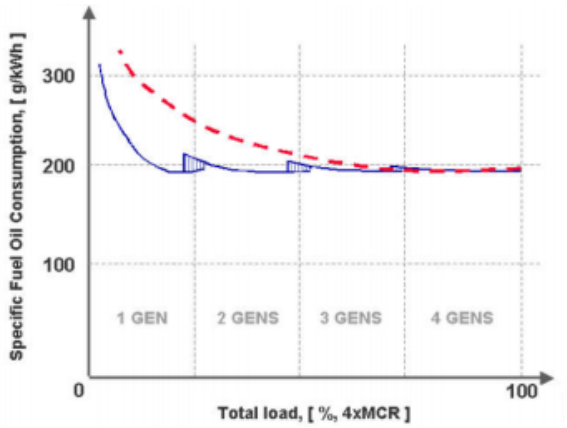

(b) Fuel consumption of multiple gensets (blue) vs. that of a single genset (red).

Figure 2.1: Example fuel oil consumption of medium speed diesel engine (Ådnanes, 2003).

To regulate the speed of the engine a governor is used, where every engine has a governor each. The governor regulates the flow of diesel to the combustion chamber. The governor was originally a mechanical system, but in modern machinery it is controlled by a computer. The governors cooperate with each other using load-sharing techniques. There are several ways of achieving load-sharing between governors, which will be discussed in section 3.1.2.

2.1.1 Dynamic characteristics

The diesel engine is often modeled as a rotating inertia with a mechanical torque given from the combustion in the cylinders. The governor is modeled as a PID controller which chases the desired shaft speed ω_d. The dynamical equation of the engine's shaft dynamic becomes

$$\dot{\omega} = \frac{1}{J}\left(\tau_m - \tau_e - D\omega\right) \tag{2.1}$$

where ω is the rotational velocity of the shaft, J is the shaft's moment of inertia, τ_m is the torque applied from the pistons, τ_e is the electric torque from the generator and D is the coefficient for linear damping.

2.2 Generator

Driven by a diesel engine, a generator converts rotational mechanical energy into electrical energy through electromagnetic forces. There are several types of generators, such as asynchronous generators, synchronous generators and DC-generators. In marine power plants a synchronous generator is typically used to produce power (Torstein I. Bø, 2015).

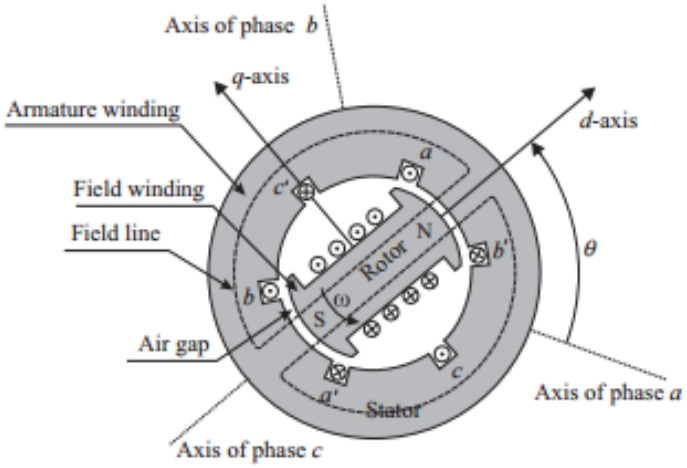

Figure 2.2: Basic build up of a synchronous generator producing a three-phase current.

The synchronous generator consist of two main components: the rotor and the stator. The rotor is the center piece of the generator. It produces a static magnetic field, either by a DC current through field windings. The stator surrounds the rotor, and consists of several electrical wind-

ings called armature windings. The magnetic field from the rotor creates an opposite magnetic field from the stator. When a prime mover forces rotation on the rotor, the magnetic field of the stator follows the rotations, and this induces a three-phase alternating current in the stator coils. The three phases produced have a 120^o phase shift with respect to each other.

The number of magnetic poles (P) in the rotor determines the relationship between the mechanical speed ω_m and the frequency f of the currents produced in the stator. By using the number of pairs of poles $p = \frac{P}{2}$ and n the rotor speed (rot/min), the frequency (Hz) of the induced current is expressed by

$$f = \frac{\omega}{2\pi} = \frac{p \cdot \omega_m}{2\pi} = \frac{(p \cdot 2\pi \cdot n)/60}{2\pi} = p \cdot \frac{n}{60} \tag{2.2}$$

The DC currents acting in the rotor windings was earlier transferred by brushes, which gives the name *brushed* to its type of generators. Some modern generators have brushless excitation of the DC currents in the rotor, for reduced downtime and maintenance. The DC current in the windings relates to the terminal voltage produced by the generator, and is used to control the voltage output.

The terminal voltage of the generator is regulated by an automatic voltage regulator (AVR) which manipulates the induced voltage of the rotor windings. The AVR uses a PID-controller to control the terminal voltage to a reference value by changing the currents in the rotor. Regulations state that the stationary voltage variation on the generator terminals are not to exceed $\pm 2.5\%$ of nominal voltage, and the largest transient load variation can not exceed -15% or 20% of nominal voltage. To satisfy these regulations, the AVR is normally equipped with a feed-forward function (Ådnanes, 2003).

2.3 Rectifier

A rectifier is an electrical device that converts AC to DC by allowing current to pass while its positive and blocking when the current is negative. For high-power applications, such as a marine power plant, three-phase current is the norm, and the topology of a three-phase rectifier is presented in figure 2.3. A pair of flow controllers is connected to each of the three-phase

lines, which only allow the current to flow in one direction. When the three-phase currents flow through these controllers, they create a rippled DC current, as can be seen in the figure.

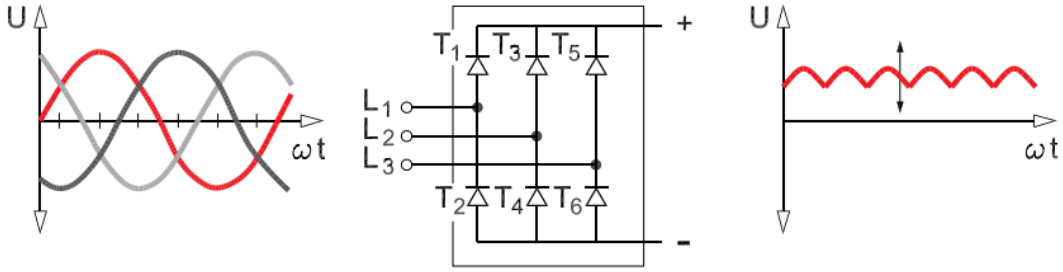

Figure 2.3: Topology of a three-phase rectifier, with three-phase AC voltage on the left and rippled DC voltage on the right.

2.3.1 Dynamic characteristics

There are multiple ways of modeling a rectifier. A high-fidelity model of a rectifier requires the high frequency switching dynamics of the flow controllers. A high-fidelity model is demanding to compute, thus a simpler model is proposed as an example. A medium fidelity rectifier can be modelled as a transformer of AC from the dq-plane directly to DC, skipping the need of three phase AC conversion and switching in the diodes. Without modelling the diodes switching, a time continuous model can be developed which significantly simplifies the system while keeping the dynamic behavior and the power transfer in the system (I. Jadric, 2002).

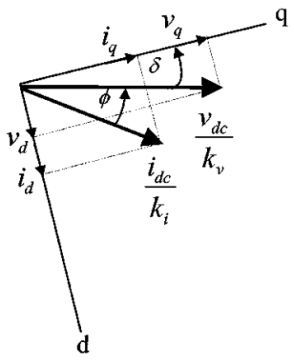

Figure 2.4: The relationship between the AC currents and voltages in the rotor dq reference frame and the rectified average DC current and voltage.

The relationship between the AC voltages and currents in the dq-plane and the average values of the rectified DC voltage and current is presented in figure 2.4. This is based on the assumption that the average value of the rectified variables is directly proportional to the fundamental

harmonics of the input AC variables (I. Jadric, 2002). From the relations given in figure 2.4 the following equations are obtained

$$i_{DC} = k_i \sqrt{i_d^2 + i_q^2} \tag{2.3}$$

$$\delta = arctan(\frac{i_d}{i_q}) - \phi \tag{2.4}$$

$$v_d = \frac{v_{DC}}{k_v} cos(\delta) \tag{2.5}$$

$$v_q = \frac{v_{DC}}{k_v} sin(\delta) \tag{2.6}$$

where the parameters k_v, k_i and ϕ are included to represent the effects of the non-ideal diode rectification. These parameters are modelled as constants, and retrieved from (I. Jadric, 2002). δ represents the angle of the synchronous generator rotor. The voltages and currents are described by their subscripts. The equations above are valid while the generator is delivering power. If the DC voltage becomes too high, the generator will start to consume power (acting as a motor), this is not physically possible due to the diodes in the rectifier not allowing power to flow in backwards direction. To avoid this unphysical behavior, the equation for v_{DC} is modified to be

$$v_{DC} = \begin{cases} v_{DC} & \text{if } v_d i_d + v_q i_q > 0 \\ i_{DC} R_{block} & \text{otherwise} \end{cases} \tag{2.7}$$

where v_{dc} is the voltage from the DC link. R_{block} is a blocking resistance of the diode, it is set to a high value to represent the blocking of the diode.

2.4 DC link

A DC link is a connection between a rectifier and an inverter. It usually consists of a combination of capacitors and inductors, which serves the purpose to smooth ripples in the DC voltage produced by the rectifier. The capacitor of the DC link is connected in parallel and inductors are usually connected in series, as seen in figure 2.5.

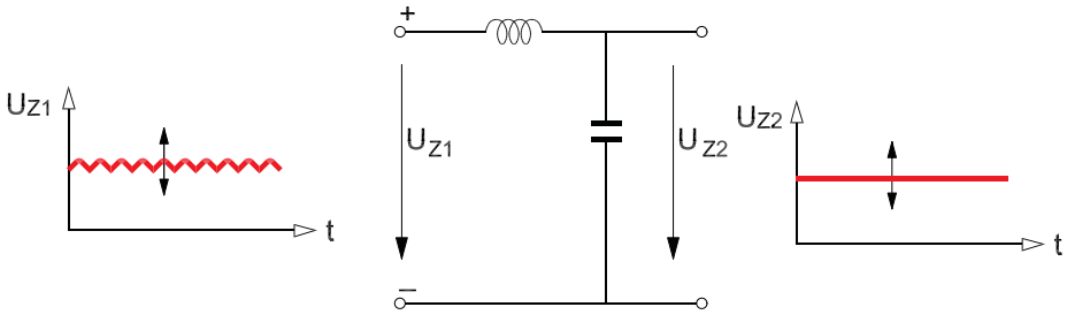

Figure 2.5: Schematic representation of a DC link with an inductor and a capacitor, and how the ripples from the rectified DC voltage are smoothed.

2.4.1 Dynamic characteristics

The DC link is often modelled as a single capacitor

$$\dot{v}_{DC} = \frac{1}{C}\sum i \tag{2.8}$$

C is the capacitance, connected as seen in figure 2.5 plus the capacitance of the filters connected to the rectifier and inverter. The current for a component is positive when it is delivering power, and negative when it is consuming power.

2.5 Inverter

An inverter does the opposite of a rectifier, it converts DC current to AC current. This is done by switching on and off thyristors, as seen in figure 2.6, or by using transistors which allows for a more controllable inverter. The frequency of the AC produced by the inverter is controlled by a frequency and voltage signal from the motor controller. An AC voltage is then generated by the invertor and sent to the motor, which makes the motor create a current.

By controlling the frequency of the current produced, the inverter can set the RPM of a motor receiving the AC current. With the relation in equation 2.2, the frequency of synchronous motors receiving the AC current produced by the inverted is proportional to the frequency of the AC current, thus making the inverter a great component for controlling the speed of motors.

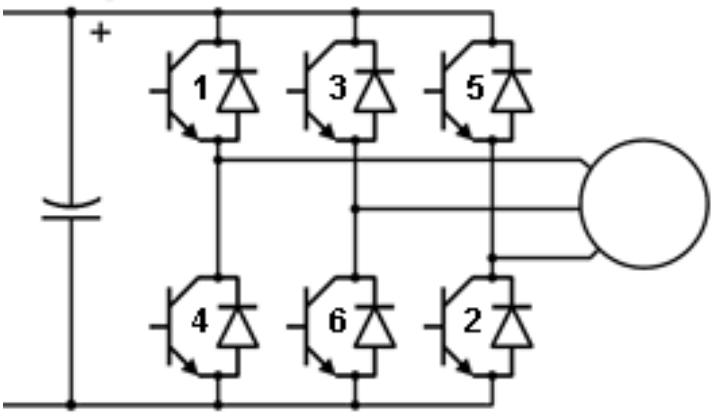

Figure 2.6: Schematic representation of a thyristor based inverter connected between a dc link and a motor.

The smoothness of the inverted AC current is dependent on the switching frequency of the thyristors. The higher the switching frequency the smoother the produced current become, this happens at a cost of efficiency, as there is a minor loss in every switching operation. The effect of switching frequency can be seen in figure 2.7.

2.5.1 Dynamic characteristics

A high-fidelity model of an inverter includes the high frequency switching dynamics of the transistors used, such a high-fidelity model is similar to one of a rectifier. An alternative to this high-fidelity model is a steady power relation through the inverter, which greatly simplifies

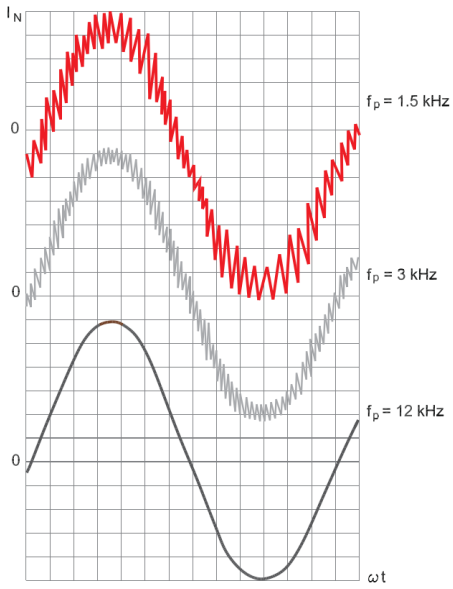

Figure 2.7: Schematic representation of a thyristor based inverter connected between a dc link and a motor.

the model. The equation given below greatly simplifies what happens in an actual inverter, as switching frequency and transistor dynamics are not included. The model assumes a smooth inverted AC current, and a constant efficiency of the inverter. The DC voltage is given by the capacitor in the DC link, and the DC current can be found by the following power balance equation.

$$v_{DC} i_{DC} \cdot \eta_{inv} = v_{AC} i_{AC} \tag{2.9}$$

In reality the efficiency of an inverter is not fixed, as it is in this model. This is a simplification of the dynamical properties of the thyristors or transistors used in marine power plants.

2.6 Motor

A motor converts electrical energy into mechanical rotational energy. The most common types of motors on board vessels are synchronous motors and induction motors. A synchronous motor is identical to a synchronous generator, but instead of being actuated by the rotation of a shaft, the actuation comes from an incoming three-phase AC voltage.

2.7 Energy storage device

An energy storage device (ESD) is capable of providing or consuming power on demand. There are different ways of achieving this, one can store energy in a rotating mechanical object called a flywheel, or the energy can be stored electrochemically in a battery or as a pure electrical charge in a super-capacitor. This thesis will focus on the rechargeable lithium-ion battery.

Different terms are used in describing battery states and behaviors. State of charge (SOC) is a percentage of how charged a battery is between empty (zero) and full (100%). Depth of discharge (DOD) is a measure of the range of SoC is used when charging and discharging a battery. The battery voltage is the voltage measured over the battery. This voltage is dependent on the battery's state of charge, and whether the battery is charging or discharging, as shown in figure 2.8.

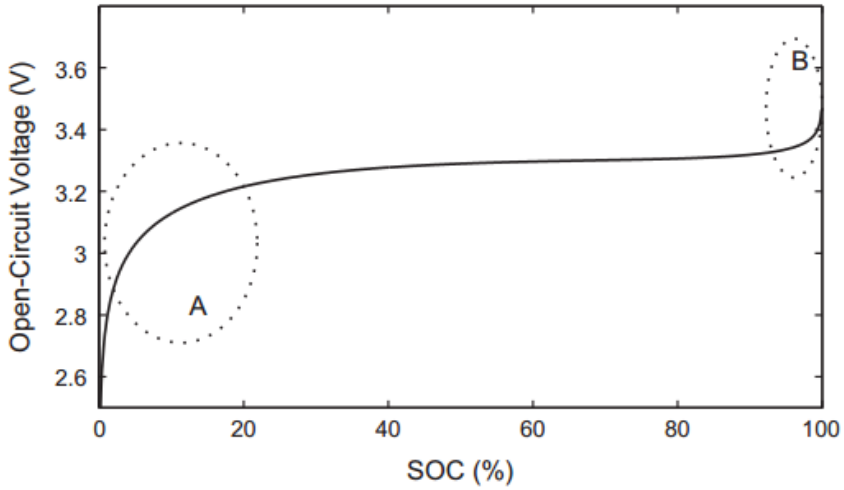

Figure 2.8: Charge- and discharge voltages of a battery.

One of the biggest challenges with using rechargeable lithium batteries in the industry is the battery's durability. Over time, the batteries are subjected to loss in both energy and power capability. The rate of degradation is dependent on operating conditions such as battery temperature, SOC, voltage, DOD, and current magnitude are the most influential aging factors (T. Waldmann, 2014). The effects of degradation in a battery is loss of capacity and an increase in internal resistance (Issam Baghdadi, 2016).

The degradation of batteries are mainly separated into two main reasons; calendar ageing and cycle degradation. Both degradations are results of chemical reactions, which will not be studied

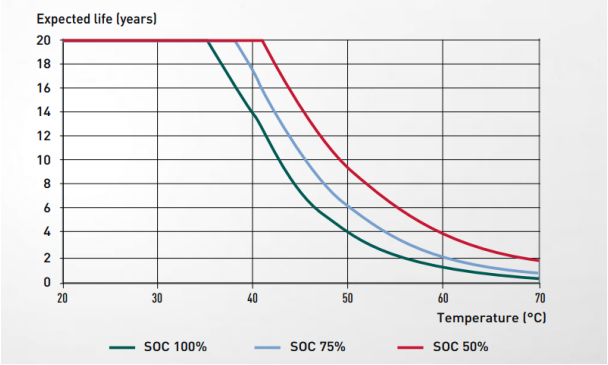

Figure 2.9: Expected calendar life according to temperature. Curtesy of Saft Batteries.

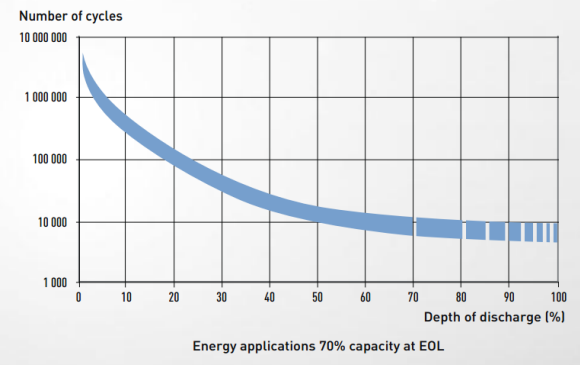

Figure 2.10: Expected cycle life of a battery as a function of DOD. Curtesy of Saft Batteries.

in this thesis. Calendar ageing occurs whether or not a battery is used. As shown in figure 2.9, the temperature of the battery has a significant effect on its lifetime, and the battery's SoC also effects its lifetime. Cyclic ageing only occurs if the battery is in use, and is dependent on the number of charge-discharge cycles the battery has been exposed to, and the DOD for each cycle.

2.7.1 Dynamic characteristics

A high-fidelity model of a lithium-ion battery describes the chemical reactions in the battery (Zhang, 2011). A simpler model is presented as an example where the dynamical characteristics of the battery is as a controlled voltage source model in series with a resistance (Olivier Tremblay, 2007), as shown in figure 2.11.

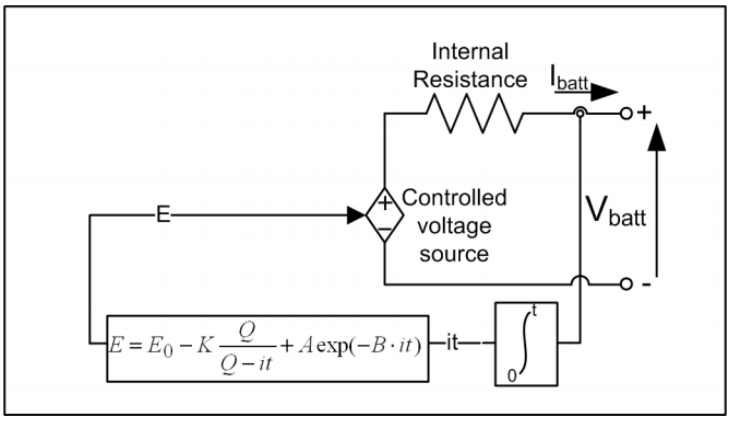

Figure 2.11: Non-linear battery model (Olivier Tremblay, 2007)

The current drawn from the battery is dependent on the difference between battery no-load voltage E and the battery voltage $Vbatt$ as can be seen in equation 2.11. Equation 2.10 shows how the no-load voltage changes based on the battery's current charge.

$$E = E_0 - K\frac{Q}{Q - \int i\,dt} + A\,exp(-B \cdot \int i\,dt) \tag{2.10}$$

$$V_{batt} = E - R \cdot i \tag{2.11}$$

The proposed model a medium fidelity battery model, and there are several specific assumptions and limitations to its design, many of which are based on (Olivier Tremblay, 2007).

1. Model assumptions
    - The model's parameters are deduced from the discharge characteristics and it is assumed to be the same for charging.
    - Temperature does not affect the battery's behavior.
    - There is no Self-Discharge in the battery.
    - Memory effects are neglected in the model.
    - Degradation of the battery is neglected.
2. Model limitations
    - Minimum battery voltage is $0V$ and the maximum voltage is not limited.
    - Minimum capacity is $0Ah$ and the maximum capacity is not limited.

Without limitations in maximum voltage or capacity, the model needs a supervisory control. This is called a battery management system, which monitors the states of the battery. The battery management system is further discussed in section 3.3.

2.8 DC Breaker

In a multiterminal DC system (MTDC) where multiple sources and consumers supply and draw power from the DC link, one must be able to isolate single systems in case of a fault. The DC breaker acts as a protection relay which disengages a faulty system from the active MTDC, by not allowing any current through (R. K. Mallick, 2011).

The regular breaker simply stops current from passing through when tripped. Most commonly a IGBT semiconductor is used which has the ability to conduct or stop current in one direction. By implementing two IGBT's mirrored to each other, one is able to break current in both directions as shown in figure 2.12.

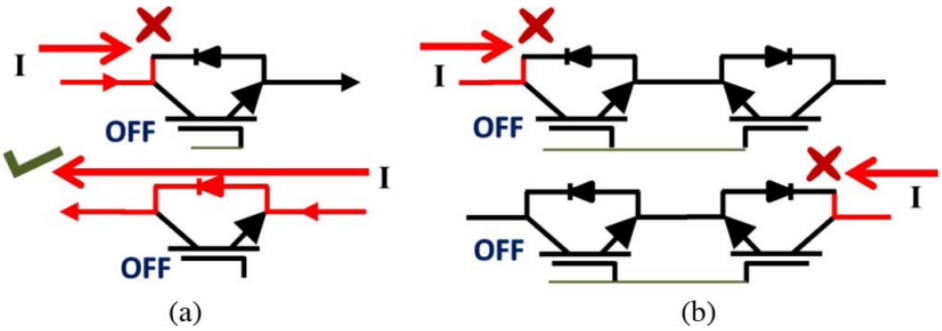

Figure 2.12: (a) Single IGBT breaker is unable to break current in reverse direction.
(b) Mirrored pair of IGBT breakers breaks current in both directions (Umer Amir Khan, 2015).

Compared to an AC breaker, the DC breaker needs to break at a much higher current which makes the operation more demanding. As the AC current naturally crosses zero current twice every wave, making the AC breakers operation one of timing, the DC breaker disengages while there is a large current passing through it (Umer Amir Khan, 2015). This effect is shown in figure 2.13. This effect results in much larger and more expensive breakers for DC grids, compared to AC grids.

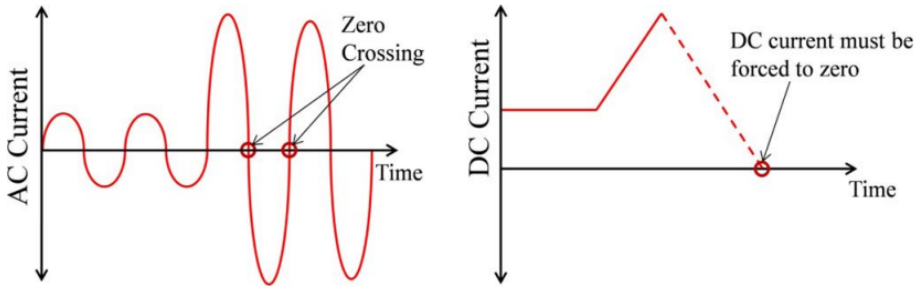

Figure 2.13: AC and DC current behavior when a fault occurs.

2.9 DC-DC converter

A DC-DC converter converts DC from one voltage level to another. The DC-DC converter is mainly used to connect batteries and superconductors to the electrical grid. It gives a level of control over the energy storages, and is a necessity in energy storage systems where batteries are used. The converter allows control of charging and discharging a battery.

Typical efficiencies for a DC-DC converter are 94%-96% while operating at optimum loadings (Woo-Young Choi, 2011). The efficiency is highly dependent on how large the transformation of the voltage is, as a larger transformation or lower power throughput leads to lower efficiencies.

2.9.1 Dynamical characteristics

The model used to describe the converter assumes a constant efficiency of the inverter. The model of the converter is described by a steady power relation through the DC-DC converter. The power loss is modeled as a constant efficiency for currents in both directions through the converter, and for both increasing and decreasing the voltage. The equation below describes how the power from one side of the converter relates to the other.

$$P_1 = \eta_{dcdc} \cdot P_2 \tag{2.12}$$

$$v_1 i_1 = \eta_{dcdc} \cdot v_2 i_2 \tag{2.13}$$

In reality the efficiency of an inverter is not fixed, as it is in this model. This is a simplification of the dynamical properties of the thyristors or transistors used in marine power plants.

Chapter 3

Power and Energy Management Systems

In a marine electrical power plant the various parts of the automation system controls their respective parts of the power system. Even though the components are separated, they are all interconnected by the power distribution system. Control of the power system is essential for safe operation while minimizing fuel consumption. A supervisory energy control system is needed to monitor all the components in the power system.

The function of the Power Management System (PMS) is to ensure that there is a sufficient amount of available power for the actual operational condition (Ådnanes, 2003). Available power is defined as the rated power of the system subtracted by the consumed power. The information about the operating condition is obtained by monitoring the load status of the generator sets and the power system. If the available power drops too low, the PMS will handle it by starting up a new generator if there is anyone available, otherwise the PMS can reduce the load demand by shutting off consumers. Removing consumers from the grid is called load-shedding. One can extend the functionality of a power management system to include monitoring and control of the energy flow in a way that utilizes the equipment with optimal fuel efficiency, such systems can be called Energy Management System (EMS) (Ådnanes, 2003).

According to (Ådnanes, 2003) the main functions of the PMS and EMS can be separated into three groups.

- Power generation management:
  Overall control and monitoring of generator frequency and voltage, active and passive

load sharing monitoring and control, and load dependent start stop of generator sets.

- Load management:
  Monitoring of the load power and coordinator of power limitations in other systems, load shedding and start interlock of heavy consumers based on the current available power. Start interlock is when a heavy power consumer is put on hold by the PMS until the available power is large enough to handle the heavy consumer.
- Distribution management:
  Configuration and sequence control of the power distribution. The requirements in the vessels operational modes shall be met by the distribution system.

A blackout is considered the worst-case scenario for a vessels electrical system. A blackout is defined as a total loss of electric power generation. Without power generation, the vessel loses propulsion and manoeuvrability. If the blackout is not restored as quick and safe as possible there is a severe risk for human, environmental and economic damages. The PMS or EMS main task is to prevent a blackout from occurring and maintaining the operational ability of the vessel.

There can be several different causes for blackouts, among them are reverse power due to governor failing or AVR, single component failure, diesel-generator trip, overloads and short-circuits. If the PMS can stop these failures from happening or hindering failures from propagating through the system, then blackouts will be prevented.

3.1 Load Control and Overload Protection

When the total electrical demand exceeds the electrical capacity of the power plant, an overload occurs. The engines are forced to work above their rated power to supply the demand from the consumers. After one engine fails the other engines will share its load, causing domino-effect of shut-downs through the other running engines as they also are overloaded. This leads to a blackout of the electrical system, and must be prevented (Ådnanes, 2003).

The main task of the PMS in load control is to start new generators when the demand has increased past a threshold, this is known as load dependent start and stop of gensets. The objective is to ensure that the load is supplied by an appropriate number of generators. A new

generator is activated after the power demand have exceeded a limit for a configurable period. A start-up table, as shown in table 8.1, defines the power- and time limits. There can be multiple load limits with their own time periods for each number of generators running. The first limit is usually at a lower load limit with a high time demand, while the other might cover more critical scenarios where the load limit is set to close to maximum and the time limit is low. There are different start-up tables for different operational modes, as some operations are more critical and demand more available power at any given time.

	Start 1		Start 2	
No. gensets	Load	Time	Load	Time
1	40	10	98	1
2	55	10	98	1
3	68	10	98	1
4	80	10	98	1
5	84	10	98	1

Table 3.1: Load dependent start table with two starting points for each number of gensets. The table does not include a load dependent stop function.

If the desired demand exceeds the power supplied by the generators, a load shedding is started by the PMS. Load shedding means that the least important consumers are not prioritized. This allows for the most vital consumers to remain active, and prevents a blackout by reducing the load on the gensets.

As load shedding is a method where the PMS is reactive to overload, one wishes a more proactive PMS where the overload situation never happens in the first place. By implementing start interlock for heavy consumers, one can hold off heavy power consumers until there is enough available power to support them. This method allows the PMS to know the future power demand of the system, and not allow heavy consumers to cause overloads in the system.

3.1.1 Synchronization

This section is based on chapter 7 in (Woodward).

Synchronization is the matching of the voltage wave from an AC generator with that of another AC system (Woodward). The synchronization is normally applied to the component generating the electricity, as it simpler to control. There are five conditions that must match for two systems

to be considered synchronized.

- Number of phases in each system
- The direction of rotation of the phases
- The voltage amplitudes of the systems
- The frequencies of the systems
- The phase angle of the voltages

The number of phases in each system (Figure 3.1) and the direction of rotation of the phases are determined by the configuration and specifications of the equipment, and must be a match in order to achieve synchronization.

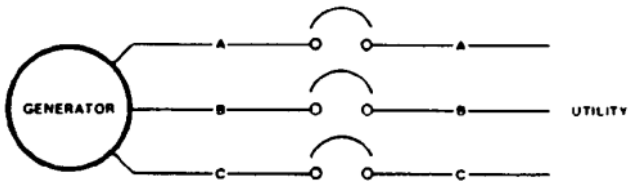

Figure 3.1: The number of phases must match in generator and utility. (Figure from (Woodward))

Before paralleling two generators the voltages generated should be within $1-5\%$ of eachother. The voltage produced by a synchronous generator is controlled by its AVR. If the voltage amplitude between two synchronous generators are not properly matched the generated voltage will not match either of the generators, as shown in Figure 3.2. This difference will result in reactive currents and a reduced system efficiency.

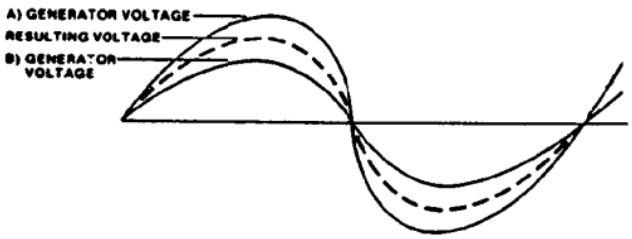

Figure 3.2: Voltage differences in two connected generators with the resulting voltage produced. (Figure from (Woodward))

In the case of synchronous generator connected to a larger system, the voltage differencing before connecting would not change the voltage on the bus, as shown in figure 3.3. This will

change the power factor of the generator, and if the voltage difference is sufficiently large the generator could be motored, i.e consume power from the bus.

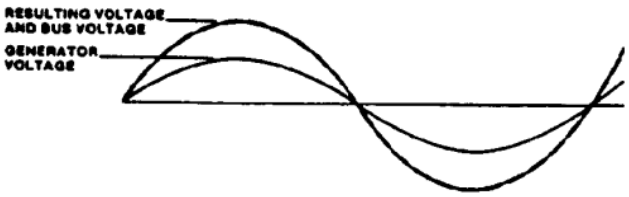

Figure 3.3: Voltage differences in two connected generators with the resulting voltage produced. (Figure from (Woodward))

The frequency of the systems being connected must be close to the same, usually within 0.2% of eachother. The frequency is normally matched by controlling the speed of the prime mover. A difference in frequency would quickly cause the phase to come out of sync, as shown in Figure 3.4.

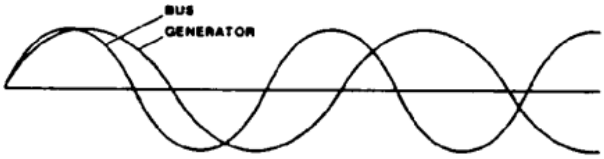

Figure 3.4: Difference in frequency. (Figure from (Woodward))

The phase of a generator must match the bus before connecting to it, normally within ±10 degrees. For synchronous generators the phase is matched by controlling the prime mover. A short temporary drop or increase in frequency would respectively increase or decrease the phase of the generator. Figure 3.5 show a larger phase of the generator than the bus, the prime mover would need to speed for a short amount of time to match the phase of the bus.

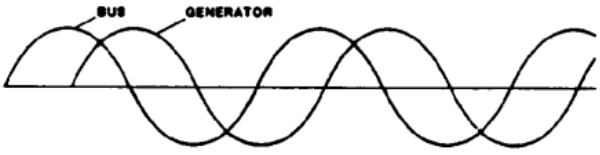

Figure 3.5: Difference in phase. (Figure from (Woodward))

3.1.2 Load-sharing

An isolated system is an application where multiple engines are driving a common load. The load might be a propeller or pump, but most commonly the load are electrical generators con-

nected to a power grid.

In an isolated system, there is a need for a load-sharing strategy. Without a proper strategy in a system with two engines with slightly different speed settings will end up with one engine taking all the load and the other will shed its load, as the coupled system must have a single speed. The governors will adjust the fuel rate of each engine to reach its desired speed, but the engines will end up fighting against each other and only one will end up supplying power to the load.

Isochronous load-sharing allows for gensets to communicate with each other and prevent instabilities in the system. A load-sharing line is connected between the gensets, called a *load-sharing line*. This line consists of two conductors whereas the voltage difference between the wires represent the output power as a percentage of rated power produced by each of the gensets. If a genset power differs from that of the load-sharing line, it adjusts its speed to change its produced power to fit the load-sharing line.

Droop

A governor controlled engine might become unstable when subjected to a sudden change in loading. An increased load acting on the engine results in the engine speed to slow down. The governor then increases the fuel input to accelerate the shaft to the reference speed ω_{ref}. Due to the inertia of the shaft the governor overshoots the reference speed and responds by reducing the fuel input to decelerate the shaft causing an undershoot. This system becomes unstable for rapid changes in load.

By implementing droop the engine speed becomes stable, as droop adjusts the reference speed ω_{ref} when the load changes (Woodward). Thus stabilizing the system for large load changes. Droop is given in percent of original frequency change from no-load to full load, droop is normally set to 3-5%. From the desired load frequencies, the droop can be calculated as proposed below.

$$Droop = \frac{\omega_{no-load} - \omega_{full-load}}{\omega_{full-load}} \cdot 100 \tag{3.1}$$

Where the no-load and full-load frequencies corresponds to the desired shaft frequency at zero power and rated power, respectively. The droop adjusted reference speed can be expressed as

$$\omega_{ref} = \omega_{no-load} - \frac{P_g}{P_r} \cdot Droop \tag{3.2}$$

Where P_g is the power currently delivered by the generator to the grid, and P_r is the generators rated power. The resulting droop curve is shown in figure 3.6, where the droop no load-frequency is illustrative put at 60 and 63 Hz and the full-load frequency is 57 and 60 Hz, respectively. The Figure shows how the droop curve can be moved to a desired frequency at a given percentage loading.

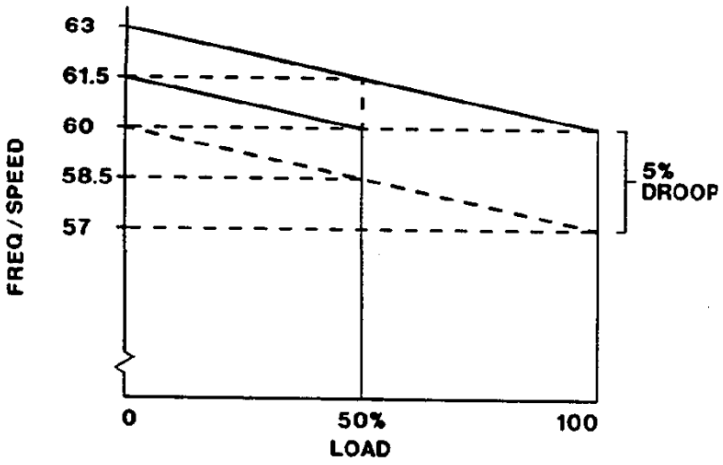

Figure 3.6: Example of droop curves constant 5% droop and different no-load frequencies.

The error given to the PID for minimizing is a comparison between the updated reference frequency and the actual frequency of the shaft. The error is expressed as

$$error_\omega = \omega_{ref} - \omega \tag{3.3}$$

The schematic implementation of droop is shown in Figure 3.7, where the error is given to the governor modeled as a PID controller, which controls the fuel injection to the engine modeled as a torque.

If all engines in a system have the same droop setting, they will share load proportionally (Woodward). The load carried by each engine is dependent on their speed settings. A change in engine load causes the engines frequency to change. The droop handles the issue where governors chase the engine speed to where one engine carry all the load. If a certain ratio between

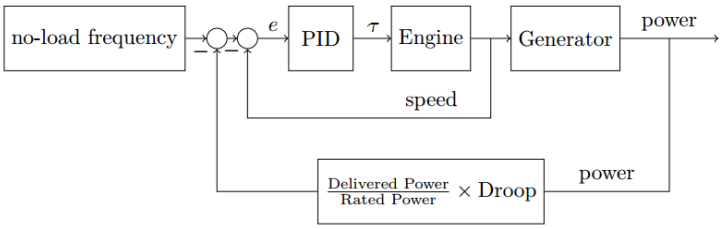

Figure 3.7: Schematic overview of droop implementation. (Figure from (Bø, 2012))

the gensets produced power can also be acquired by adjusting the droop setting.

The main disadvantage with using droop is that the speed of the shaft changes as the load changes. A way of counteracting this effect is to modify the droop curve to achieve the actual desired shaft speed. Most often it is not necessary to adjust the droop, as the 3-5% change in frequency due to load variations is acceptable.

3.1.3 Load-up ramp and deload ramp

Loading up and deloading generators after connecting or before disconnecting to the bus makes the power system operate smoothly without any sudden changes load sharing. The goal is to have generators producing zero power bus when being connected to or disconnected from the bus. This can be achieved with droop control, by moving ω_{nl}, the no load frequency, to match the frequency of the bus.

When a genset is being disconnected from the bus, its no load frequency is continuously decreased to match the frequency of the bus. Decreasing the no load frequency causes the generator to produce less and less power down to zero produced power when the no load frequency matches the frequency of the bus. The power produced has now been distributed among the other generators connected to the bus. The deloaded genset is now free to disconnect causing sudden power spikes in the other gensets.

After connecting a genset its power is ramped up to equally match that of the other generators. After the genset has been synchronized to the bus with regards to frequency, phase and voltage, it is connected. Now the no load frequency of the generator is matching the frequency of the bus, which means that the genset produces no power. The no load frequency is increased

to match that of the other generators to ensure an equal load sharing. Figure 3.8 show the droop curves of two gensets when genset2 is ready to be connected or disconnected from the bus.

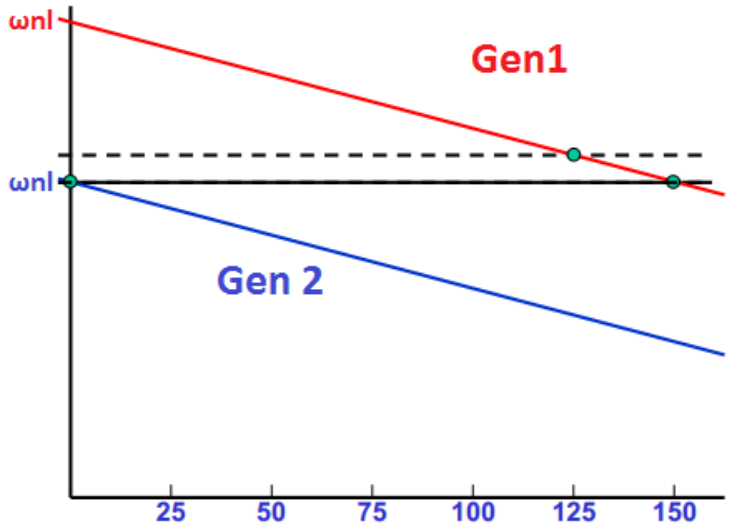

Figure 3.8: The droop curves of two generators in a load sharing operation. Gen 2 is currently producing no load as its no load frequency matches that of the bus. (Modified Figure from TMR4290 lecture 7.)

3.2 Short-circuit protection

A short circuit is a low resistance contact between the two conductors supplying electrical power in a circuit. This connection is most often unintended, and allows for excessive amount of current to flow through the new circuit, often leading to equipment being burned. In a marine electrical system a short-circuit in usually defined as a worst-case single failure, as the consequence of it is the loss of the component or the distribution grid where the short-circuit happened.

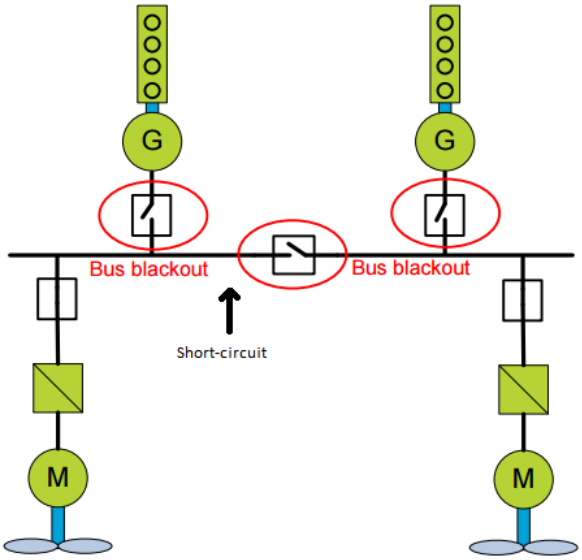

Figure 3.9: Protection relays trigger after a short-circuit causes a full blackout. (Figure made by Dr.Ing Olve Mo, Marine Cybernetics.)

To prevent the short-circuit currents from damaging the power equipment, protection relays are used to disconnect different parts of the electrical grid. A protection relay is a breaker set to open when a short-circuit is detected. As shown in Figure 3.9, triggering the protection relays causes a blackout on both the buses, leading to a full blackout.

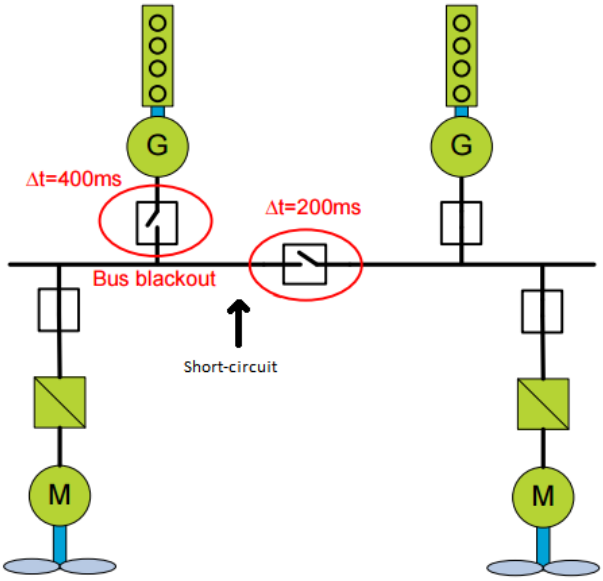

Figure 3.10: Protection relays with selectivity only causes one bus to blackout. (Figure made by Dr.Ing Olve Mo, Marine Cybernetics.)

By using protection relays with selectivity, one can prevent them from causing full blackouts onboard. With a different delay (selectivity) in each protection relay, the bus tie breaker is set

to trigger first, isolating the faulty bus from the functioning one, causing only a partial blackout where only one bus is out of operation. The effect of selectivity in protection relays is shown in Figure 3.10, where the breaker connected to the right generator does not trip, as it is set to trip at $400ms$ but is being cut off from the short-circuit after $200ms$.

Using protection relays with selectivity does not prevent short-circuits from occurring, but does prevent a full blackout. The PMS is monitoring the currents, if a large current spike is detected, the correct relays must be triggered.

3.3 Battery Management System

One of the biggest challenges with using lithium-ion batteries in hybrid solutions on-board vessels is the battery's limited lifetime. Due to relatively high investment costs, ship owners are interested in hybrid solutions with battery solutions that lasts for more than a few years. To increase the lifetime of batteries, one must prevent misuse of the battery. As discussed in section 2.7, battery degradation is highly dependent on parameters such as temperature and DOD. Misuse of the battery may result in a drop of the battery's state of health (SoH).

By implementing a Battery Management System (BMS) a level of control of the battery pack is introduced. With the ability to monitor the states of the battery, one can significantly increase its lifetime by operating the battery within its ideal conditions. The main monitoring tasks of the BMS is to detect battery voltage and cell temperatures Yinquan Hu (2015).

While some states are directly measurable other states such as the battery's state of charge (SOC) and its SoH are not, and must therefore be estimated by the BMS. Knowing the SoC of the battery is integral in understanding the DOD the battery is exposed to J.N. Hu (2014). With a correct estimate of the SOC one can ensure that the battery is operated at optimal conditions, which prevents misuse and limits degradation of the battery.

3.3.1 State of Charge estimation

The United States Advanced Battery Consortium defines the SOC of a battery to be the ratio of the remaining charge (C_r) to the normal charge (C_n) (J.N. Hu, 2014). The SOC is represented as a percentage, as expressed in the equation below.

$$SOC = \frac{C_r}{C_n} \cdot 100\% \tag{3.4}$$

There are multiple ways of estimating battery SOC. The most straightforward method is open circuit voltage (OCV) measurement. The estimated SOC based on OCV can be assumed to be true when there is a linear relation between OCV and SOC. As shown in Figure 2.8, the relationship is only somewhat linear inside ~ 10% to ~ 90% SOC. Even inside this linear area, the relationship may be effected by external conditions such as temperature Yinjiao Xing a (2014). Also, to be able to accurately measure the OCV, the battery can not be at a working state. This is a limitation of the OCV method, as the SOC needs to be estimated in real time while operating the battery.

Another method for SOC estimation is the current integral method (Kong Soon Ng, 2009) which is widely used in a variety of battery systems. The current integral method constantly collects and integrates the current. As for all processes where a measurement is integrated, if there is an error in the measurement the accumulation of this error would lead to a drift off of the SOC estimation. Even though the method is easy to implement, one must ensure an accurate measurement of the current. One proposed way of estimating SOC from current integral is to develop a learning method which via learning the non-linear relationship from factors such as charge-discharge rate and battery temperature Yao He (2013). As correct continuous measurements are crucial for a proper SOC estimation using the current integral method, this method allows for SOC estimation also while the battery is operating, which makes the current integral method more viable for hybrid marine power plants than the OCV method.

Chapter 4

Hybrid Dynamical Systems

A hybrid dynamical system is described as a system that can be expressed in the following form Goebel (2012).

$$\begin{cases} x \in C & \dot{x} \in F(x) \\ x \in D & x^+ \in G(x) \end{cases} \tag{4.1}$$

Where x is the state vector, $\dot{x}$ represent the velocity of the state vector and x^+ represent the value of the state vector after an instantaneous change. The expression suggests that the state x of the hybrid system can change according to a differential inclusion $\dot{x} \in F(x)$ while in the set C, and while in the set D the state can change according to a difference inclusion $x^+ \in G(x)$. This way of expressing a hybrid system allows for discrete jumps (in D) in a otherwise continuous environment (in C).

The behavior of dynamical systems that can be described by a differential inclusion is referred to as *flow*, and the behavior of dynamical systems that can be described by a difference inclusion is referred to as *jumps* (Goebel, 2012). From this terminology a set of names for the objects in equation 4.1 are used.

By using the model in equation 4.1 one can capture the dynamics of continuous-time systems or discrete-time systems on $\mathbb{R}^n$. The continuous-time system corresponds to a flow set equal to $\mathbb{R}^n$ with an empty jump set, while the discrete-time system corresponds to a empty flow set and a jump set equal to $\mathbb{R}^n$. A system which has both continuous-time and discrete-time properties

C	*flow set*
F	*flow map*
D	*jump set*
G	*jump map*

Table 4.1: Terminology in hybrid dynamical systems.

can be expressed by setting the flow set and the jump set equal to $\mathbb{R}^n$.

Chapter 5

Modelling of a Marine Power Plant as a Hybrid Dynamical System

The marine power plant model is based of the *Marine Vessel and Power Plant System Simulator* from (Ingebrigtsen Bø, 2016).

5.1 Power Plant Model

5.1.1 Generator model

Marine power plants generally uses synchronous generators driven by diesel engines as power producers. When rotational power is converted to electrical power the generator set experiences an electrical torque, which is modeled as

$$\tau_e = \frac{p + p_{loss}}{\omega} = \frac{p}{\omega} + \frac{r(p^2 + q^2)}{\omega v^2} \tag{5.1}$$

where ω is the frequency of the shaft (rad/s), p and p_{loss} is the active power generated and the active power loss in the generator, r is the stator winding resistance, q is the reactive power and v is the teminal voltage. The terminal line voltage of the first phase is given as

$$\tilde{V}_a = -Z\tilde{I}_a + \tilde{E}_a \tag{5.2}$$

where Z is the impedance of the genset, $\tilde{I}_a$ is the current through phase a and $\tilde{E}_a$ is the induced line voltage for phase a. The magnitude of $\tilde{E}_a$ is controlled by the AVR and is expressed as

$$\tilde{E}_a = \omega \cdot V_f, \tag{5.3}$$

where V_f is the AVR controlled field voltage. The per phase angle of $\tilde{E}_a$ is expressed as

$$\angle \tilde{E}_a = \frac{\theta N_{poles}}{2} \tag{5.4}$$

where θ is the mechanical angle of the shaft, and N_{poles} is the number of poles in the generator.

Governor

The governor is based on droop control (Woodward), as introduced in section 3.1.2. The governor consists of a PID regulator that calculates fuel input to the engine based on a desired angular velocity of the shaft. The integrator term contains an anti wind-up to prevent the bias from increasing during saturation of fuel input (Torstein I. Bø, 2015). The equations for describing the governor are given as

$$\omega_{ref} = \omega_{NL} - Droop_{gen} p \tag{5.5}$$

$$u = K_p(\omega_{ref} - \omega) + K_i \xi - K_d \dot{\omega} \tag{5.6}$$

$$\dot{\xi} = \omega_{ref} - \omega + K_b(u_{saturated} - u) \tag{5.7}$$

$$\omega_{nl} = 1 + 0.5 \cdot Droop_{gen}, \tag{5.8}$$

where K_p, K_i, K_d and K_b are the proportional, integration, derivative and back-calculation gain, respectively. $Droop_{gen}$ is the droop value and p is the per unit generator active power. ω_{ref} and ω_{NL} are the reference frequency and the no-load frequency.

Automatic Voltage Regulator

The AVR is used to regulate the terminal voltage by changing the field voltage in the rotor windings. A droop controller is used to determine the setpoint, based on the reactive power of the generator set. This ensures that multiple generators connected to a bus deliver an equal amount of reactive power given that they have equal voltage droop curves (Torstein I. Bø, 2015). A simple PI controller is implemented to regulate the field voltage. The equations for the AVR are

$$\dot{V}_f = \frac{V_f - V_{avr}}{T_{avr}} \tag{5.9}$$

$$\dot{\xi}_{avr} = V_{f,ref} - |V_t| \tag{5.10}$$

$$V_{f,ref} = V_{nl}(1 - q_{gen} \cdot Droop_{avr}) \tag{5.11}$$

$$V_{avr} = K_p(V_{f,ref} - |V_t|) + K_i \xi_{avr} \tag{5.12}$$

$$V_{nl} = 1 + Droop_{avr} \cdot 0.5, \tag{5.13}$$

where V_f, V_{avr}, and $V_{f,ref}$ are the low passed field voltage, the unfiltered field voltage and the reference field voltage in the rotor windings, K_p and K_i are the proportional and integration gain. ξ_{avr} represent the integral bias in the PI controller. V_{nl} and $Droop_{avr}$ are the voltage no-load and the droop of the AVR. The reactive power produced by the generator is denoted q_{gen} and T_{avr} is the low pass filter time constant for the AVR.

The low pass filter is included to prevent an algebraic loop, it has no function except this, and the time constant is set to a low value to minimize the effect of the filter on the AVR.

Shaft speed dynamics

The shaft is modeled as a rotating inertial body with a mechanical angle. The equations for the shaft are

$$\dot{\delta} = \omega_b(\omega - \omega_0), \tag{5.14}$$

$$\dot{\omega} = \frac{1}{2H}(-D_f\omega + \tau_m - \tau_e), \tag{5.15}$$

where δ is the angle between the induced line voltage E and the angle of the bus voltage V_{bus}, ω and ω_0 represent the per unit angular velocity of the shaft and the electrical bus. ω_b is the base frequency. τ_m is the per-unit mechanical torque applied by the engine, τ_e is the per-unit electric load torque and D_f is the windage friction constant. H is defined as

$$H = \frac{1}{2} \cdot \frac{J\omega_b^2}{P_b} \tag{5.16}$$

where the rotational inertia of the generator set is denoted J and P_b is the base power of the generator set (Torstein I. Bø, 2015) & (Krause et al., 2002).

5.1.2 Bus model

Thevenin equivalent circuit

The voltage of the bus is needed to calculate the load sharing of the generator sets (Torstein I. Bø, 2015). If there are more than one generator connected to the bus, they are connected to in parallel as shown in figure 5.1.

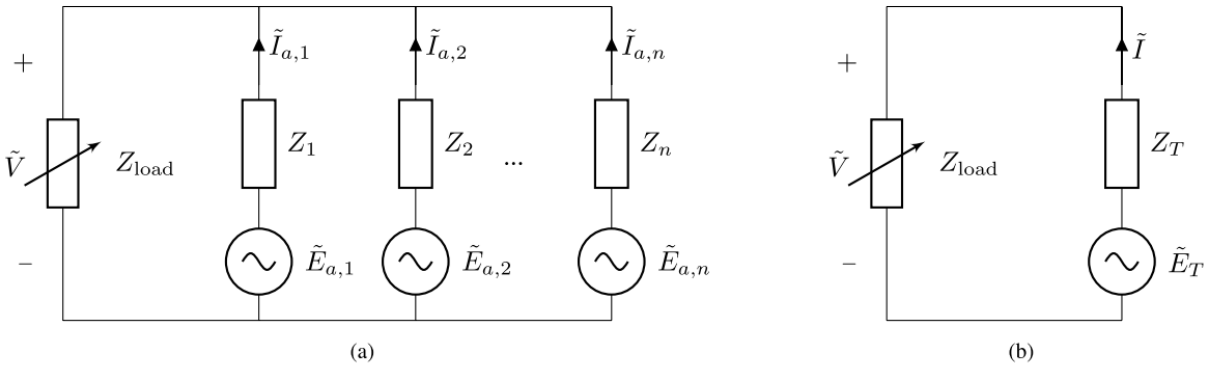

Figure 5.1: (a) Circuit diagram of bus with one load with the impedance Zload and n generators. (b) Thevenin equivalent circuit of (a). Curtesy of (Torstein I. Bø, 2015)

Thevenin equivalent circuit of the generators are used to represent the all connected generators as one circuit with only a impedance and a voltage source. The Thevenin equivalent impedance is obtained by using equation 5.17 for equivalent impedance of parallel networks which is given by combining kirchoff's first law and Ohm's law (Bird, 2007).

$$Z_t = \sum_{i=1}^{n} \left(\frac{1}{Z_i}\right)^{-1} \tag{5.17}$$

The Thevenin equivalent voltage is calculated by using superposition. The Thevenin voltages from each of the voltage sources are calculated and summed as shown in equation 5.18, to find the circuits equivalent Thevenin voltage, E_t (Bird, 2007).

$$E_t = \sum_{i=1}^{n} \frac{E_i}{Z_i} \cdot Z_t \tag{5.18}$$

Bus voltage calculation

The voltage of the bus is needed to calculate the load sharing of the generators (Torstein I. Bø, 2015). The loads on the bus are assumed to be independent of the bus voltage, making both their active and reactive power given. The thevenin voltage and impedance are calculated from equations 5.17 and 5.18, respectively. This gives the equation

$$P_{bus} + Q_{bus} = 3\tilde{V}I^* = 3\tilde{V}\frac{E_t^* - \tilde{V}^*}{Z_t^*}, \tag{5.19}$$

where P_{bus} and Q_{bus} are the active and reactive loads acting on the bus, $\tilde{V}$ is the bus voltage, E_t and Z_t are the Thevenin equivalent voltage and impedance, and I is the current through the bus. The star notation on e.g. E_t^* indicates the conjugation of the complex number.

By dividing equation 5.1.2 into a real and an imaginary part one obtain two equations with two unknowns, the real and imaginary part of the bus voltage. Equation 5.1.2 can be rewritten as

$$P_{bus} \cdot Real(Z_t^*) = Real(3\tilde{V}I^* Z_t^*) \tag{5.20}$$

$$Q_{bus} \cdot Imag(Z_t^*) = Imag(3\tilde{V}I^* Z_t^*). \tag{5.21}$$

Equation has either two, one or zero solutions depending on the load on the bus. This is illustrated in Figure 5.2. For situations with two solutions the solution with the largest absolute value is selected, as the largest voltage yields a high resistance of the load which gives a low current, hence a low internal loss. The lowest voltage solution gives a load resistance smaller than the Thevenin equivalent resistance. This causes a high current with most of the voltage drop over the internal impedance which causes a high internal loss (Ingebrigtsen Bø, 2016).

It may occur that there exist no solution of equation 5.1.2. This may happen during a rapid increase of load or a sudden decrease of the Thevenin equivalent voltage produced by the generators, this may be a result of a sudden disconnect of a generator or a fault in the AVR.

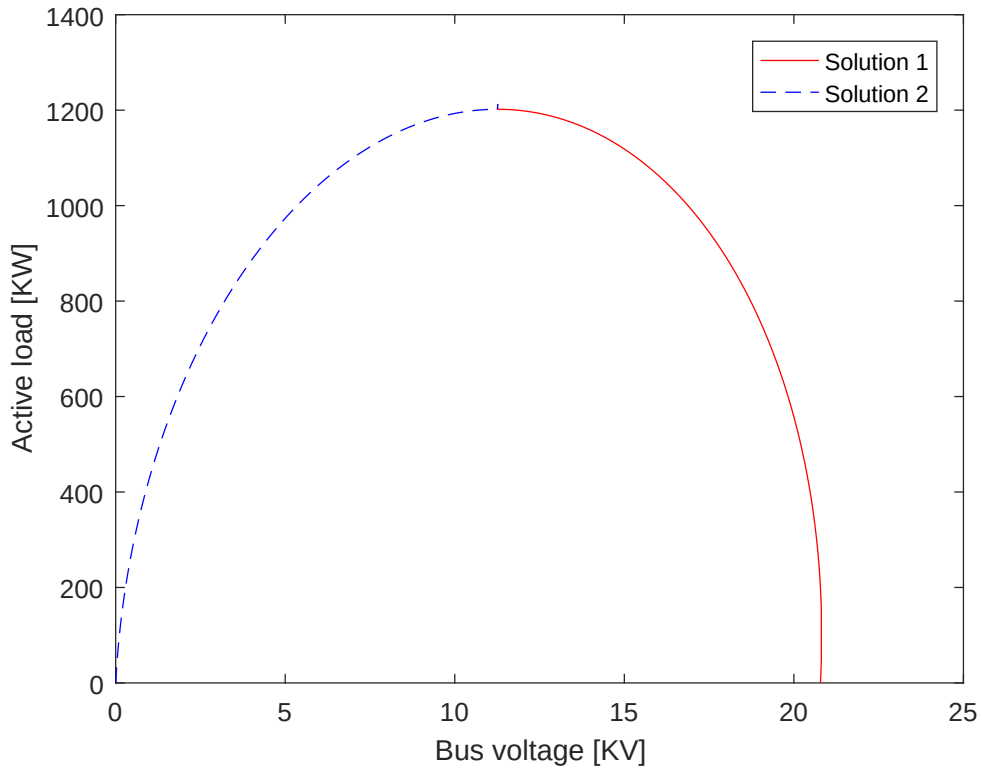

Figure 5.2: Illustrative solution of the real bus voltage for different active load on the bus. Note that the size of the curve changes with the Thevenin equivalent voltage.

5.2 Load control with Start/Stop table

A start/stop table is implemented to adapt the number of running generators to the power demand from the bus. The start/stop table checks if the average load, p_{avg} on the generators is above or below the predefined load and timer of the current number of connected gensets.

The current number of connected gensets are expressed as n. And for n active gensets the average power supplied by the generator sets is given by the following equation (Skjetne, 2016).

$$p_{avg} = \frac{1}{n}\sum_{i=1}^{n} p_i \tag{5.22}$$

In the model the timers τ_L, τ_H and τ_{HH} are used (Skjetne, 2016). These timers are following the logic

$$\dot{\tau}_L \in \{0,1\}, \qquad \dot{\tau}_L \in \begin{cases} 1, & \text{if } p_{avg} \leq p_{L,n} \\ 0, & \text{else,} \end{cases} \tag{5.23}$$

$$\dot{\tau}_H \in \{0,1\}, \qquad \dot{\tau}_H \in \begin{cases} 1, & \text{if } p_{avg} \geq p_{H,n} \\ 0, & \text{else,} \end{cases} \tag{5.24}$$

$$\dot{\tau}_{HH} \in \{0,1\}, \qquad \dot{\tau}_{HH} \in \begin{cases} 1, & \text{if } p_{avg} \geq p_{HH,n} \\ 0, & \text{else,} \end{cases} \tag{5.25}$$

$$\tag{5.26}$$

where $p_{L,n}$, $p_{H,n}$ and $p_{HH,n}$ are the *low*, *high* and *highhigh* limits, respectively, from the start/stop table.

5.2.1 Disconnecting a generator set from the bus

Let Ω be a boolean variable that determines whether or not the a genset is being disconnected or not, where $\Omega = 1$ states that the genset is being disconnected. Ω is expressed as

$$\Omega = \begin{cases} 1, & \text{if } \tau_L \geq timer_L \\ 0, & \text{else,} \end{cases} \tag{5.27}$$

The process of disconnecting a genset, as described in section 3.1.3, is initiated when $\Omega = 1$. The no load frequency of the disconnecting generator is moved to the frequency of the bus to reduce the power delivered by the genset to zero. The derivatives of the no load- frequency and voltage during the disconnection process becomes

$$\dot{\omega}_{nl,n} = \Omega \cdot \alpha_{p,deload} \cdot sign(\omega_{bus} - \omega_{nl,n}) \tag{5.28}$$

$$\dot{V}_{nl,n} = \Omega \cdot \beta_{p,deload} \cdot sign(|V_{bus}| - V_{nl,n}), \tag{5.29}$$

where $\alpha_{p,deload}$ and $\beta_{p,deload}$ is the steepness of the no load- frequency and voltage deload curve.

When the active and reactive power produced by the genset being disconnected reaches 1%MCR the genset is becomes disconnected from the bus. This is expressed as

$$c = \begin{cases} 0, & \text{if } (\Omega \wedge p_n \leq 0.01 p_n \wedge q_n \leq 0.01 q_n \\ 1, & \text{else,} \end{cases} \tag{5.30}$$

where c_{n+1} is the connected/disconnected state of the genset, where 1 is connected and 0 is not connected.

5.2.2 Connecting a generator set to the bus

Let Ψ be a boolean variable that determines whether or not the genset is being connected or not, where $\Psi = 1$ states that the genset is being connected. Ψ is expressed as

$$\psi = \begin{cases} 1, & \text{if } (\tau_H \geq timer_H \vee \tau_{HH} \geq timer_{HH}) \\ 0, & \text{else,} \end{cases} \tag{5.31}$$

The process of connecting a genset to the bus is started when $\Psi = 1$. Before connecting the genset must be synchronized to the bus, the no load frequency and no load voltage is moved to match that of the bus. This is to synchronize the frequency and voltage of the generator to that of the bus. The no load frequency and voltage are during the synchronization expressed as

$$\dot{\omega}_{nl,n+1} = \Psi \cdot K_{p,\omega nl}(\omega_{bus} - \omega_{nl,n+1}) \tag{5.32}$$

$$\dot{V}_{nl,n+1} = \Psi \cdot K_{p,Vnl}(V_{bus} - V_{nl,n+1}), \tag{5.33}$$

where $K_{p,Vnl}$ is the proportional gain for the no load voltage.

The new generator set is connected to the bus when the frequency and the terminal voltage of the genset matches the bus. The expression for the gensets connected state becomes

$$c_{n+1} = \begin{cases} 1, & \text{if } \Psi \wedge \omega_{n+1} \in [0.998\omega_{bus}, 1.002\omega_{bus}] \wedge V_{n+1} \in [0.995V_{bus}, 1.005V_{bus}] \\ 0, & \text{else,} \end{cases} \tag{5.34}$$

After the genset has been successfully connected to the bus, the generators no load- frequency and voltage are steadily increased to match that of the other generators. With the generators sharing both no load frequency and droop curve, the desired load sharing is obtained where each generator produces the same percentage active power and reactive power.

Rapid changes in the system could lead to instabilities; a smooth transition of the no load-frequency and voltage are desired. A sine function is used to ramp up the no load- frequency and voltage, thus ensuring continuous accelerations $\ddot{\omega}_{nl}$ and $\ddot{V}_{nl}$.

Let $t_{ramp} = t - c_t$ denote the time from connection, where t is the simulation time and c_t is the time of connecting the genset to the bus. The equations for no load- frequency and voltage increase becomes

$$\dot{\omega}_{nl,n} \begin{cases} 0, & \text{if } \omega_{nl,n} \approx \omega_{nl,0} \\ \Psi \cdot sin\left(\frac{\pi}{2} \cdot \frac{t_{ramp}}{T_{ramp,max}}\right), & \text{else} \end{cases} \tag{5.35}$$

$$\dot{V}_{nl,n} \begin{cases} 0, & \text{if } V_{nl,n} \approx V_{nl,0} \\ \Psi \cdot sin\left(\frac{\pi}{2} \cdot \frac{t_{ramp}}{T_{ramp,max}}\right), & \text{else,} \end{cases} \tag{5.36}$$

where $T_{ramp,max}$ is used to control the time to ramp up. Note that the notation has changed from $n+1$ to n, this is a result of n being incremented due to the new genset connected to the bus. The first parts of the equations are included to prevent $\omega_{nl,n}$ from oscillating after $\omega_{nl,0}$ is reached.

5.3 Hybrid Dynamical Power Plant Model

The model is to be fitted into the hybrid equation toolbox (Sanfelice, 2016) in Matlab, which offers a framework for both the continuous and discrete nature of hybrid systems, as discussed in chapter 4. To build the model in this hybrid environment, the entire system needs to be expressed in a state space vector, $\mathbf{x}$.

The state space vector is made up of the following parameters

Bus	S_{bus}	Bus load
	Z_τ	Thevenin equivalent impedance
	E_τ	Thevenin equivalent voltage
	V_{bus}	Bus voltage
	ω_{bus}	Bus frequency
	δ_{bus}	Bus load angle
Timer	τ_L	Timer low
	τ_H	Timer high
	τ_{HH}	Timer highhigh
	t	Timer of simulation
Generator	ω	Shaft frequency
	δ	Genset load angle
	c	Genset connected
	Z	Genset impedance
	E	Genset induced line to neutral voltage
	V_t	Genset terminal voltage
	s	Genset power
	τ_e	Electrical torque
	c_t	Connection time
Governor	ω_{ref}	Shaft reference frequency
	ω_{nl}	No load reference frequency
	u	Governor control input
	ξ_{gov}	Governor integration bias
AVR	$V_{f,ref}$	AVR reference field voltage
	V_f	AVR field voltage
	V_{avr}	AVR unfiltered voltage
	ξ_{avr}	AVR integration bias
	V_{nl}	No load reference voltage

Table 5.1: The parameters of the state space vector, $\mathbf{x}$.

The hybrid environment enables modeling of both the continuous changes of the power plant and the discrete on/off configurations of the generator sets. The flow map, f, describes the slow changing properties of the system, while the jump map, g, suddenly changes in the system. The

flow set and jump set determines whether the states are to behave according to the flow map or the jump map.

5.3.1 Flow Set and Jump Set

The flow set and the jump set determines whether the flow map or the jump map should define the states of the system. For simplicity the flow set is always 1, which suggests that the system is in flow at all times. However, the jump set is given priority over the flow set, causing the HDS to perform a jump when the state vector is in the jump set.

There are three situations that require a jump to be performed: disconnecting a genset, connecting a genset and resetting a timer. The criteria for performing a disconnect and a connect are presented in sections 5.2.1 and 5.2.2. Let $T_{r,L}$, $T_{r,H}$ and $T_{r,HH}$ be boolian variables that determines if their respective timers are to be reset, the equation for T_r becomes

$$T_{r,L} = \begin{cases} 1, & \text{if } (\tau_L > 0) \wedge (p_{avg} > p_{L,n}) \\ 0, & \text{else} \end{cases} \tag{5.37}$$

$$T_{r,H} = \begin{cases} 1, & \text{if } (\tau_H > 0) \wedge (p_{avg} < p_{HH,n}) \\ 0, & \text{else} \end{cases} \tag{5.38}$$

$$T_{r,HH} = \begin{cases} 1, & \text{if } (\tau_{HH} > 0) \wedge (p_{avg} < p_{HH,n}) \\ 0, & \text{else,} \end{cases} \tag{5.39}$$

The jump set D becomes

$$D = \Big\{ \big(\Psi \wedge \omega_{n+1} \in [0.998\omega_{bus}, 1.002\omega_{bus}] \wedge V_{n+1} \in [0.995V_{bus}, 1.005V_{bus}] \big) ... \\ \vee \big(\Omega \wedge p_n \leq 0.01 p_n \big) \vee \big(T_{r,L} \vee T_{r,H} \vee T_{r,HH} \big) \Big\}$$

5.3.2 Flow Map

The derivative of the state vector is needed to describe the change of the system, and partial derivatives are used to calculate this. Many of the functions in the model are multi variable. To calculate the derivative a multi variable function $f(x, y)$ the following structure is used.

$$\frac{df(x,y)}{dt} = \frac{\partial f(x,y)}{\partial x} \cdot \frac{\partial x}{\partial t} + \frac{\partial f(x,y)}{\partial y} \cdot \frac{\partial y}{\partial t} \tag{5.40}$$

The flow map are mostly derived from the equations introduced in section 5.1. The flow map of the bus states becomes

$$\dot{S}_{bus} = F(t) \tag{5.41}$$

$$\dot{Z}_\tau = \sum_{i=1}^{n} \frac{sb_i}{Z_i} c_i \tag{5.42}$$

$$\dot{E}_\tau = \sum_{i=1}^{n} \frac{sb_i\, E_i}{Z_i} c_i \cdot \dot{Z}_\tau \ ... \tag{5.43}$$

$$+ \sum_{i=1}^{n} \frac{sb_i\, \dot{E}_i}{Z_i} c_i \cdot Z_\tau \ ... \tag{5.44}$$

$$- \sum_{i=1}^{n} \frac{sb_i\, E_i}{Z_i^2} c_i \cdot Z_\tau \cdot \dot{Z}_i \tag{5.45}$$

$$\dot{V}_{bus} = f(E_\tau, Z_\tau, S_{bus}, \dot{Z}_\tau, \dot{E}_\tau, \dot{S}_{bus}) \tag{5.46}$$

$$\dot{\omega}_{bus} = \sum_{i=1}^{n} sb_i c_i \cdot \dot{\omega}_i \tag{5.47}$$

$$\dot{\delta}_{bus} = \frac{Re(V_{bus})^{-1}}{Re(V_{bus})^{-2} Im(V_{bus})^{-2} + 1} \cdot Im(\dot{V}_{bus}) \ ... \tag{5.48}$$

$$+ \frac{Im(V_{bus})}{Im(V_{bus})^2 Re(V_{bus})^2 + 1} \cdot Re(\dot{V}_{bus}), \tag{5.49}$$

while the flow map for the generator states becomes

$$\dot{\omega} = \frac{1}{2H}(-D_f\omega + u - c \cdot \tau_e) \tag{5.50}$$

$$\dot{c} = 0 \tag{5.51}$$

$$\dot{\delta} = c \cdot \omega_b(\omega - \omega_{bus}) \tag{5.52}$$

$$\dot{Z} = Re(Z) + \dot{\omega} GenXs \cdot 1i \tag{5.53}$$

$$\dot{E} = \big(V_f cos(\delta) + V_f sin(\delta)\big) \cdot \dot{\omega} \ ... \tag{5.54}$$

$$+ \big(\omega cos(\delta) + \omega sin(\delta)\big) \cdot \dot{V}_f \ ... \tag{5.55}$$

$$+ \big(-\omega V_f sin(\delta) + \omega V_f cos(\delta)\big) \cdot \dot{\delta} \tag{5.56}$$

$$\dot{V}_t = (1-c) \cdot \sqrt{3}\dot{E} + c \cdot \dot{V}_{bus} \tag{5.57}$$

$$\dot{s} = c \cdot \Bigg(3\frac{E^* - V^*_{line}}{Z^*} \cdot \dot{V}_{line} \ ... \tag{5.58}$$

$$+ 3V_{line}\frac{E^* - 1}{Z^*} \cdot \dot{V}^*_{line} \ ... \tag{5.59}$$

$$+ 3V_{line}\frac{1 - V^*_{line}}{Z^*} \cdot \dot{E} \ ... \tag{5.60}$$

$$- 3V_{line}\frac{E^* - V^*_{line}}{Z^{2*}} \cdot \dot{Z}^* \Bigg) \tag{5.61}$$

$$\dot{\tau}_e = c \cdot \Bigg(\Big(\frac{1}{\omega} + \frac{2Re(Z) \cdot p}{\omega |V_t|^2}\Big) \cdot \dot{p} \ ... \tag{5.62}$$

$$+ \Big(\frac{Re(Z) \cdot q}{\omega |V_t|^2}\Big) \cdot \dot{q} \ ... \tag{5.63}$$

$$+ \Big(\frac{-p}{\omega^2} - \frac{Re(Z) \cdot (p^2 + q^2)}{\omega^2 |V_t|^2}\Big) \cdot \dot{\omega} \ ... \tag{5.64}$$

$$+ \Big(\frac{-2Re(Z) \cdot (p^2 + q^2)}{\omega |V_t|^3}\Big) \cdot |\dot{V}_t| \Bigg) \tag{5.65}$$

$$\dot{c}_t = c, \tag{5.66}$$

The flow map for the governor becomes

$$\dot{\omega}_{ref} = \dot{\omega}_{nl} - Droop_{gen} \cdot \dot{p} \tag{5.67}$$

$$\dot{\omega}_{nl} = \Omega \cdot \alpha_{p,deload} \cdot sign(\omega_{bus} - \omega_{nl,n}) \tag{5.68}$$

$$+ \Psi \cdot sin\left(\frac{\pi}{2} \cdot \frac{t_{ramp}}{T_{ramp,max}}\right) \tag{5.69}$$

$$\dot{u} = K_p(\dot{\omega}_{ref} - \omega) + K_i\dot{\xi}_{gov} + K_d\dot{\omega}_{gov} \tag{5.70}$$

$$\dot{\xi}_{gov} = \omega_{ref} - \omega + Kb \cdot (u_{max} - u), \tag{5.71}$$

where $\dot{\omega}_{nl}$ is calculated as described in sections 5.2.1 and 5.2.2.

while the flow map describing the AVR becomes

$$\dot{V}_{f,ref} = -V_{nl}\dot{q} \cdot Droop_{avr} \tag{5.72}$$

$$+ \dot{V}_{nl}(1 - q \cdot Droop_{avr}) \tag{5.73}$$

$$\dot{V}_f = V_f \tag{5.74}$$

$$\dot{\xi}_{avr} = V_{ref} - |V_t|, \tag{5.75}$$

$$\dot{V}_{avr} = \begin{cases} K_p(\dot{V}_{ref} - |\dot{V}_t|) + K_i\dot{\xi}_{avr} & \text{if } V_{avr} \in [V_{f,min}, V_{f,max}] \\ 0 & \text{else} \end{cases} \tag{5.76}$$

$$\dot{V}_{nl} = \Omega \cdot \beta_{p,deload} \cdot sign(|V_{bus}| - V_{nl,n})... \tag{5.77}$$

$$\Psi \cdot K_{p,Vnl}(V_{bus} - V_{nl,n+1}), \tag{5.78}$$

5.3.3 Jump map

The jump map describes how the state vector describing the power plant instantly changes as a generator set is connected or disconnected from the bus. When a genset is connected or disconnected from the bus the states of the bus are changed, which again effect all gensets connected to it. This means that all gensets must jump states according to the jump map when a single genset is connected or disconnected.

When the state vector $\mathbf{x} \in D$ due to one of the timer resets T_r only one of the timers τ_L, τ_H or τ_{HH} is reset, while the rest of the state space vector does not jump, i.e $\mathbf{x}^+ = \mathbf{x}$.

Given that $\mathbf{x} \in D$ not because of a timer reset, the following jump map is used. With Sb_{bus} as the base power of the bus, and sb as a vector containing the per unit base power of each genset. The jump map of the bus states become

$$S_{bus}^{+} = S_{bus} \tag{5.79}$$

$$Z_{\tau}^{+} = \Big(\sum_{i=1}^{m} sb_i \cdot \omega_i\Big)^{-1} \tag{5.80}$$

$$E_{\tau}^{+} = \Big(\sum_{i=1}^{m} \Big(sb_i \frac{E_i^{+}}{Z_i^{+}}\Big) E_{\tau}^{+} \tag{5.81}$$

$$V_{bus}^{+} = f(E_{\tau}^{+}, Z_{\tau}^{+}, Sb_{bus}, P_{bus}, Q_{bus}) \tag{5.82}$$

$$\omega_{bus}^{+} = \sum_{i=1}^{m} sb_i \cdot \omega_i \tag{5.83}$$

$$\delta_{bus}^{+} = atan\Big(\frac{Re(V_{bus}^{+})}{Im(V_{bus}^{+})}\Big), \tag{5.84}$$

The timers reset after a genset is connected or disconnected, or when the derivative of the counter is equal to zero. The jump map of the timers become

$$\tau_L^{+} = \{0, \tau_L\} \tag{5.85}$$

$$\tau_H^{+} = \{0, \tau_H\} \tag{5.86}$$

$$\tau_{HH}^{+} = \{0, \tau_{HH}\} \tag{5.87}$$

$$t^{+} = t, \tag{5.88}$$

The jump map of the genset states are dependent of whether the genset is connected or not after the jump has been made, some jumps has two solutions as a result of this. The jump map for the genset states becomes

$$\omega^+ = \omega \tag{5.89}$$

$$c^+ \in \{0, 1\} \tag{5.90}$$

$$\delta^+ \in \{0, \delta\} \tag{5.91}$$

$$Z^+ = Re(Z) + \omega GenXs \cdot 1i \tag{5.92}$$

$$E^+ = \omega V_f cos(\delta^+) + \omega V_f sin(\delta^+) \tag{5.93}$$

$$V_t^+ \in \left\{\sqrt{3}E^+, V_{bus}^+\right\} \tag{5.94}$$

$$s^+ \in \left\{0, \sqrt{3}V_t^+ \frac{\sqrt{3}E^{+*} \cdot V_t^{+*}}{\sqrt{3}Z_\tau^{+*}}\right\} \tag{5.95}$$

$$\tau_e^+ \in \left\{0, \frac{p^+}{\omega} + \frac{Re(Z^+) \cdot (p^{+2} + q^{+2})}{\omega^+ V_t^{+2}}\right\} \tag{5.96}$$

$$c_t^+ = \Psi \cdot t, \tag{5.97}$$

where $GenXs$ is the p.u. synchronous reactance of the generator, and p and q are the active and reactive power of the genset.

The states of the governor and the AVR are modelled as fully continuous. The jump map for the governor becomes

$$\omega_{ref}^+ = \omega_{ref} \tag{5.98}$$

$$\omega_{nl}^+ = \omega_{nl} \tag{5.99}$$

$$u^+ = u \tag{5.100}$$

$$\xi_{gov}^+ = \xi_{gov}, \tag{5.101}$$

and the jump map for the AVR becomes

$$V_{f,ref}^{+} = |V_t^{+}| \tag{5.102}$$

$$V_{avr}^{+} = V_{avr} \tag{5.103}$$

$$V_f^{+} = V_f \tag{5.104}$$

$$\xi_{avr}^{+} = \xi_{avr} \tag{5.105}$$

$$V_{nl}^{+} = \frac{|V_t^{+}|}{1 - q^{+} \cdot droopAvr}, \tag{5.106}$$

Chapter 6

Power Plant Model Verification

The model, described in chapter 5, is tested in the processes of disconnecting and connecting a genset to the bus is illustrated by performing two simple simulations with the parameters given in Tables 6.1 and 6.3. The goal of the simulations are to show how the disconnection and connection processes introduced in sections 5.2.1 and 5.2.2 behaves when simulated.

6.1 Disconnecting Genset from Bus

The parameters of the simulation are presented in Table 6.1. A two genset configuration is chosen, $n_0 = 2$, where the average power of the generators is $p_{avg} = 0.15$, which is less than the low power limit of two generators connected, $p_{L,2}$. This will cause timer τ_L start counting from the beginning of the simulation.

Variable	Value	Unit
n_0	2	[-]
Gen_{sb}	10	[MW]
$Pbus$	3	[MW]
$Qbus$	1	[MW]
$\tau_{Lim,L,2}$	5	[s]
$p_{L,2}$	0.275	[p.u]

Table 6.1: Parameters for simulation of genset being disconnected.

6.1.1 Results

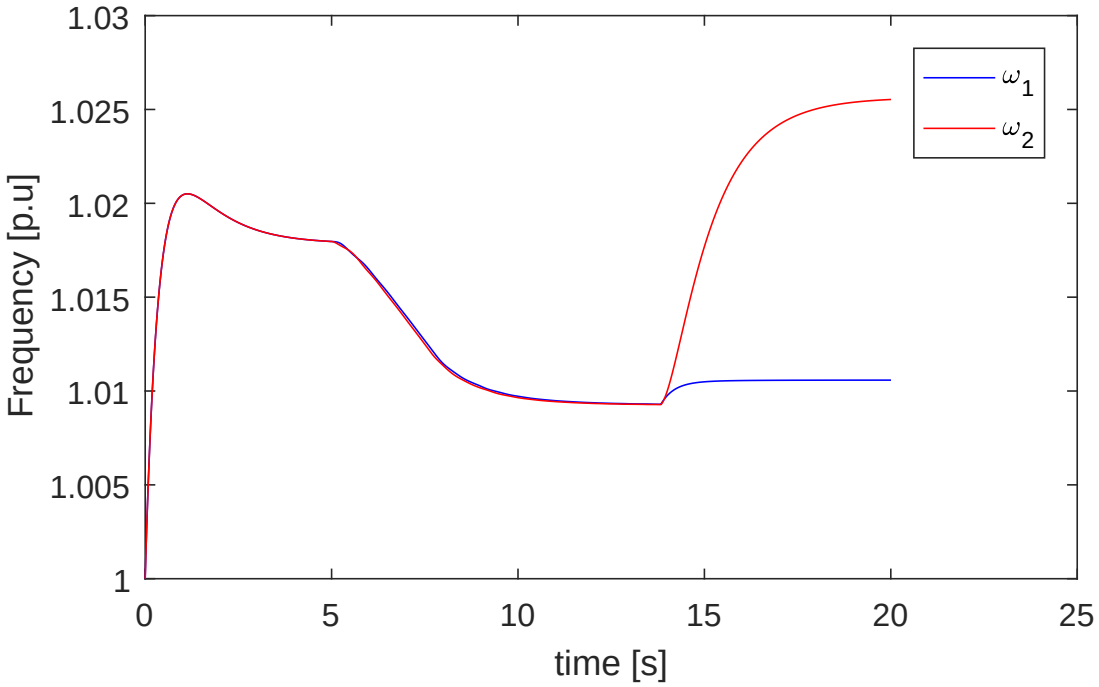

Figure 6.1: The shaft frequency of the two gensets in a disconnection operation. Changes in frequency are caused by the droop configuration.

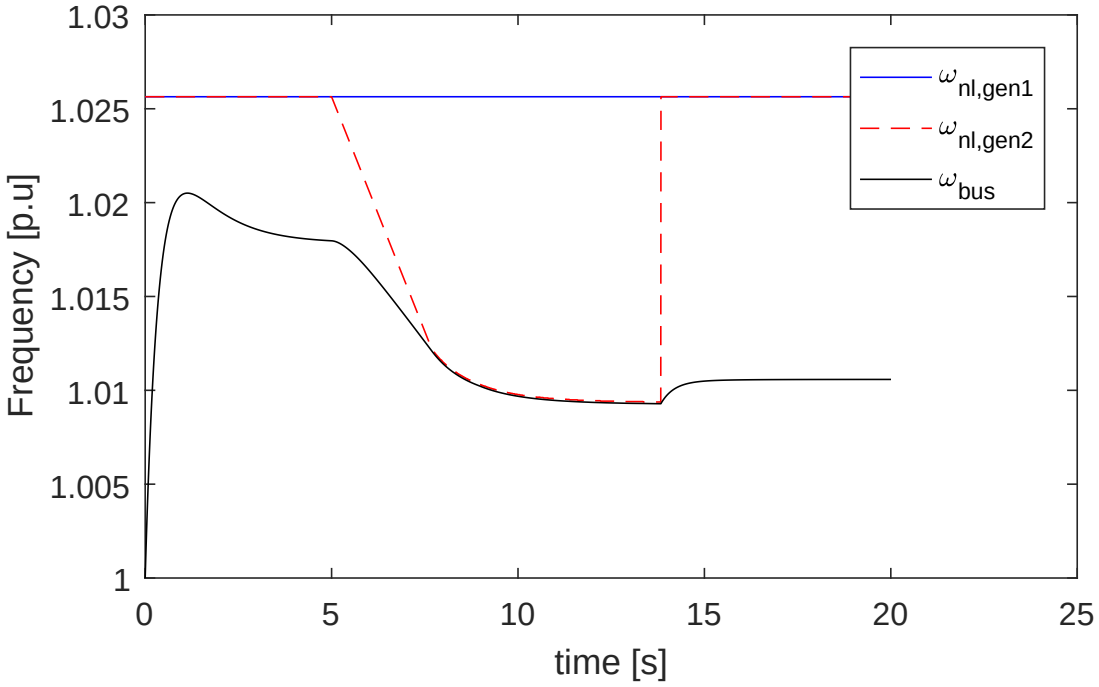

Figure 6.2: The behavior of the no load frequency of genset 2, synchronizing to the frequency of the bus, and jumping back to its initial value after genset 2 is disconnected.

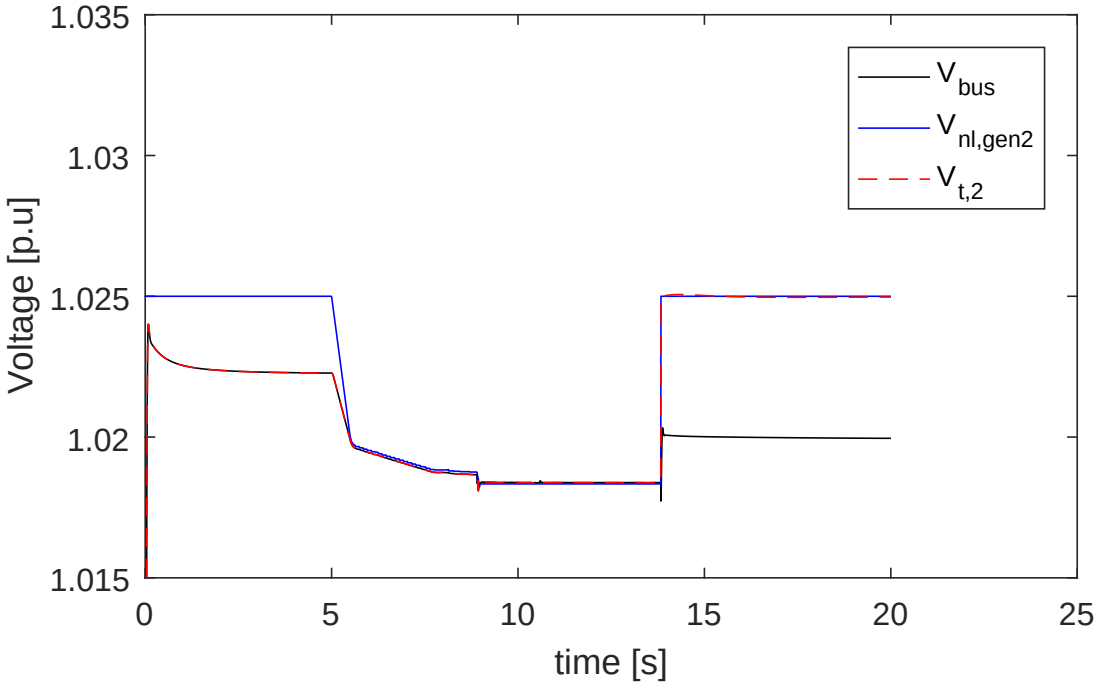

Figure 6.3: The no load voltage of genset 2 synchronizing to the bus voltage.

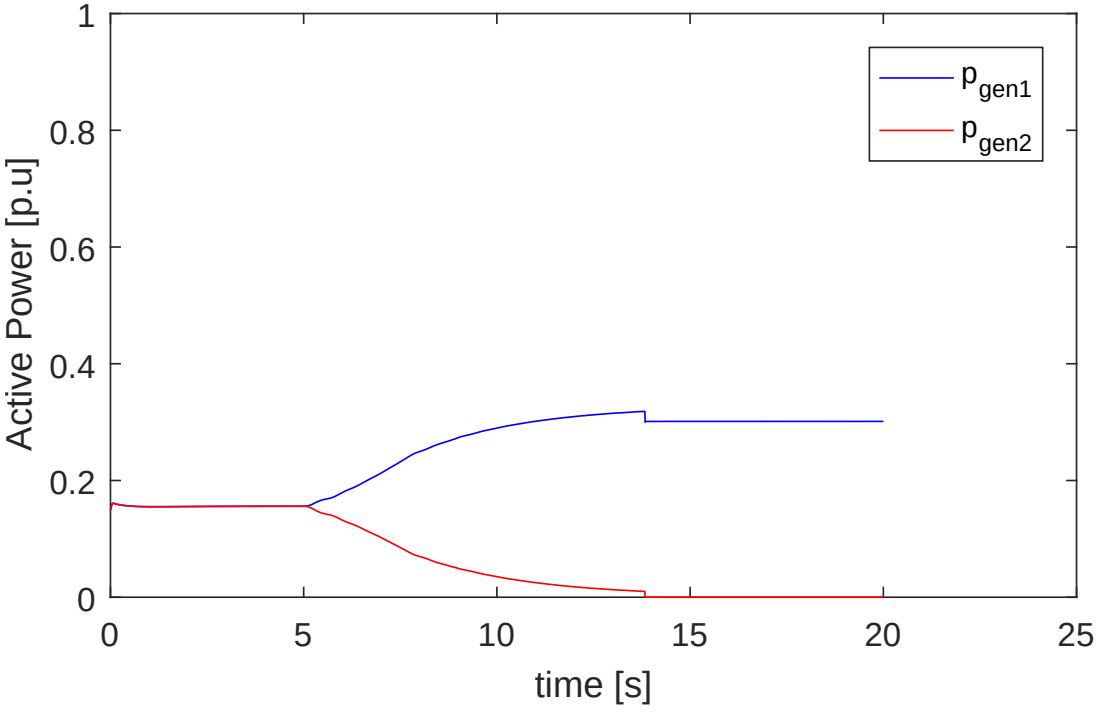

Figure 6.4: The active power of the two gensets being ramped before genset 2 is disconected from the bus.

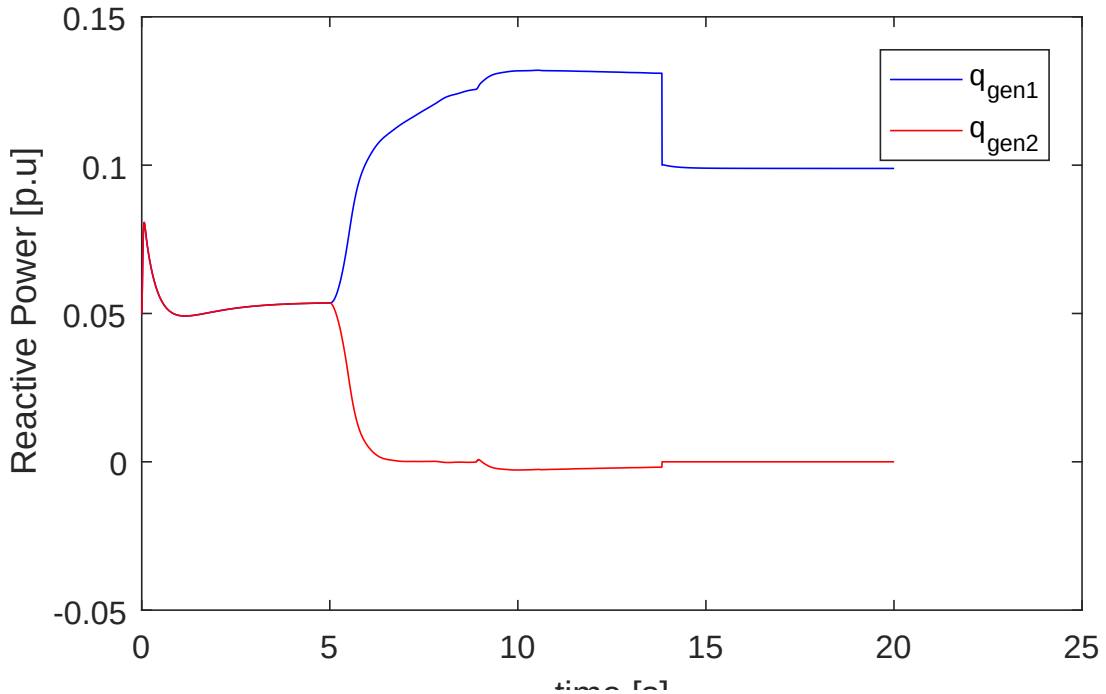

Figure 6.5: The reactive power of the two gensets being ramped before connecting to the bus.

6.1.2 Discussion

For the first 5 seconds of the simulation both gensets are connected with equal active and reactive load sharing, as can be seen in Figures 6.1, 6.4 and 6.5. After 5 seconds, the timer, τ_L, reaches the timer low limit, $\tau_{Lim,L,2}$, which sets $\Psi = 1$ and initiates the disconnection process. This causes the no load frequency and voltage of genset 2, $\omega_{nl,2}$ and $V_{nl,2}$ to ramp down to match the frequency and voltage of the bus, as can be seen in Figures 6.2 and 6.3. Reducing the no load frequency and voltage causes the active and reactive power produced by the genset 2 to be gradually overtaken by genset 1, as shown in Figures 6.4 and 6.5. When active power delivered by genset 2 reaches 1%MCR ($0.01[p.u]$) the genset is disconnected from the bus. The no load frequency and voltage of genset 2 is jumped up to its initial state.

With genset 1 operating alone, its power produced should follow the equation $S = \frac{S_{bus}}{n \cdot Gen_{sb}}$, which gives $S = 0.3 + 0.1i[p.u.]$. Just before disconnection, the power delivered by genset 1 are not at the correct level. This becomes apparent in Figures 6.4 and 6.5 with both the active and the reactive power in genset 1 overshooting its value of 0.3 and $0.1[p.u.]$ respectively. This is solved by jumping p_{gen} and q_{gen} of the connected gensets to their correct values. A similar approach is done for the induced line to neutral voltage E.

6.2 Connecting a Genset to the Bus

The process of connecting a genset to the bus is illustrated by performing a simple simulation with the parameters given in Table 6.3. The goal of the simulation is to show how the connection process from section 5.2.2 behaves in the model.

Variable	Value	Unit
Gensets connected	1	[-]
Gen_{sb}	10	[MW]
Pbus	8	[MW]
Qbus	1	[MW]
$\tau_{Lim,H,2}$	4	[s]
$p_{H,2}$	0.60	[p.u]

Table 6.2: Parameters for simulation of genset being connected.

6.2.1 Results

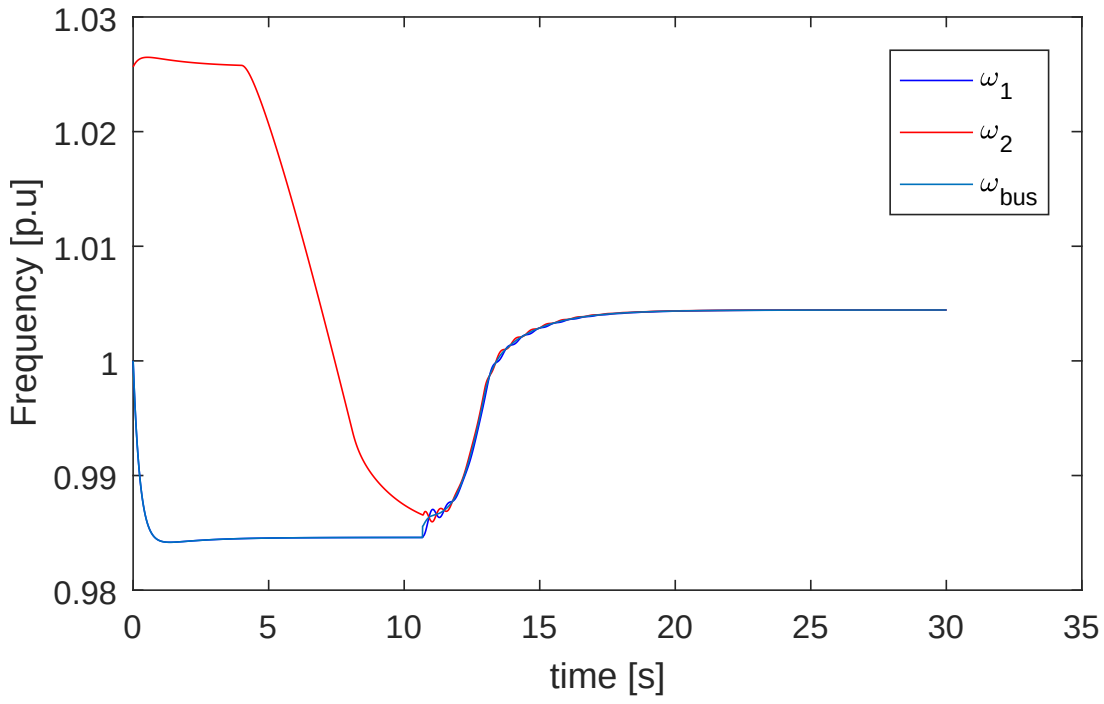

Figure 6.6: The shaft frequency of the two gensets in a connection operation. Changes in frequency are caused by the droop settings.

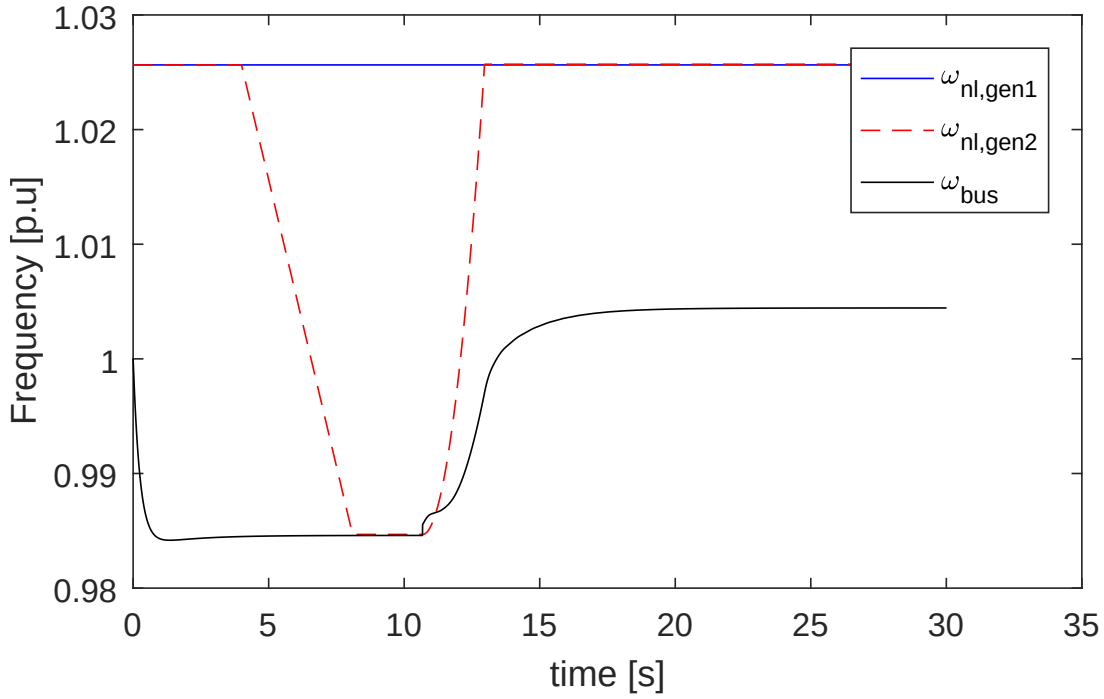

Figure 6.7: The synchronization of the no load frequency of genset 2, and ramping up in a connection operation.

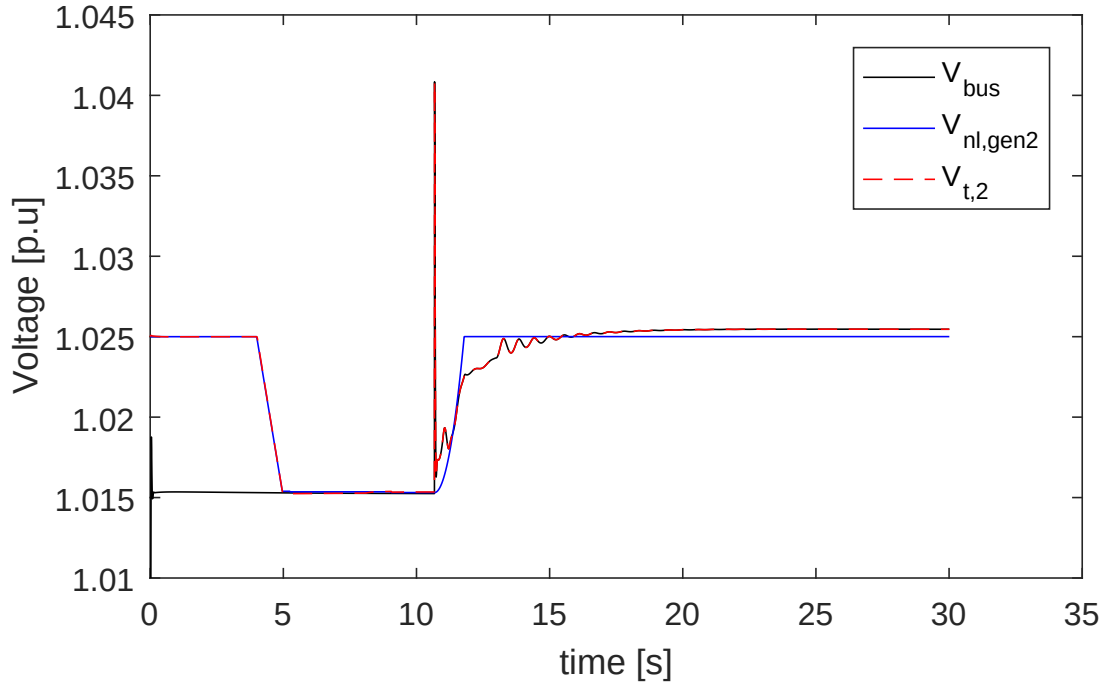

Figure 6.8: The no load voltage of genset 2 synchronizing to the bus and ramping up in a connection operation.

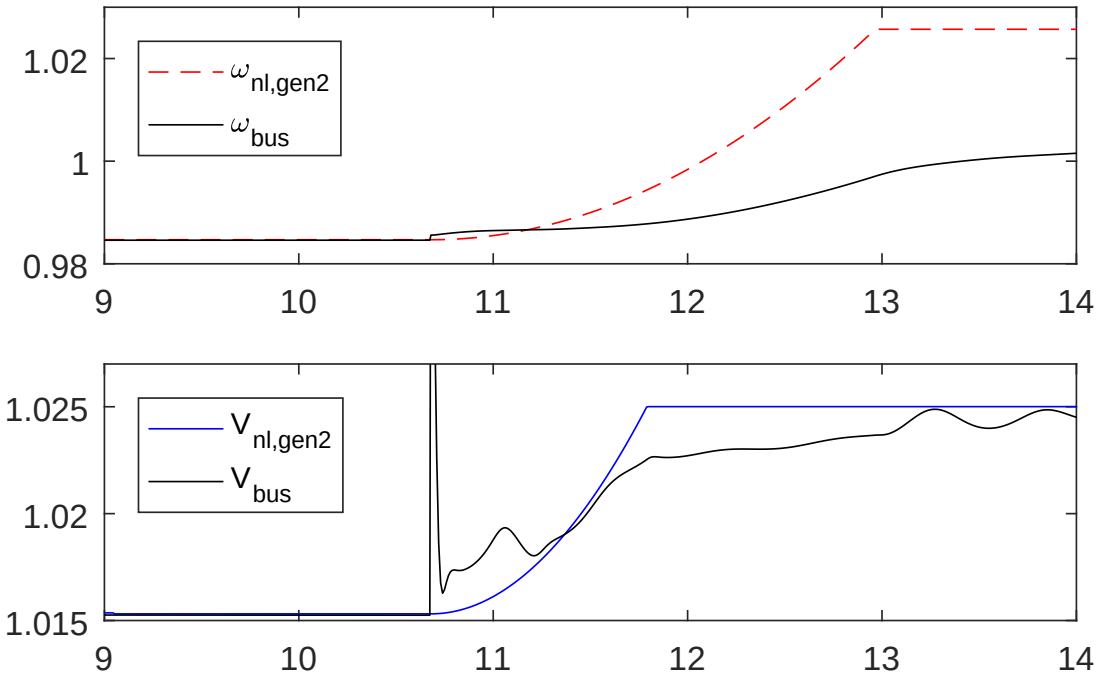

Figure 6.9: Close up of the no load frequency and voltage ramp after connection. (Figures 6.7 and 6.8).

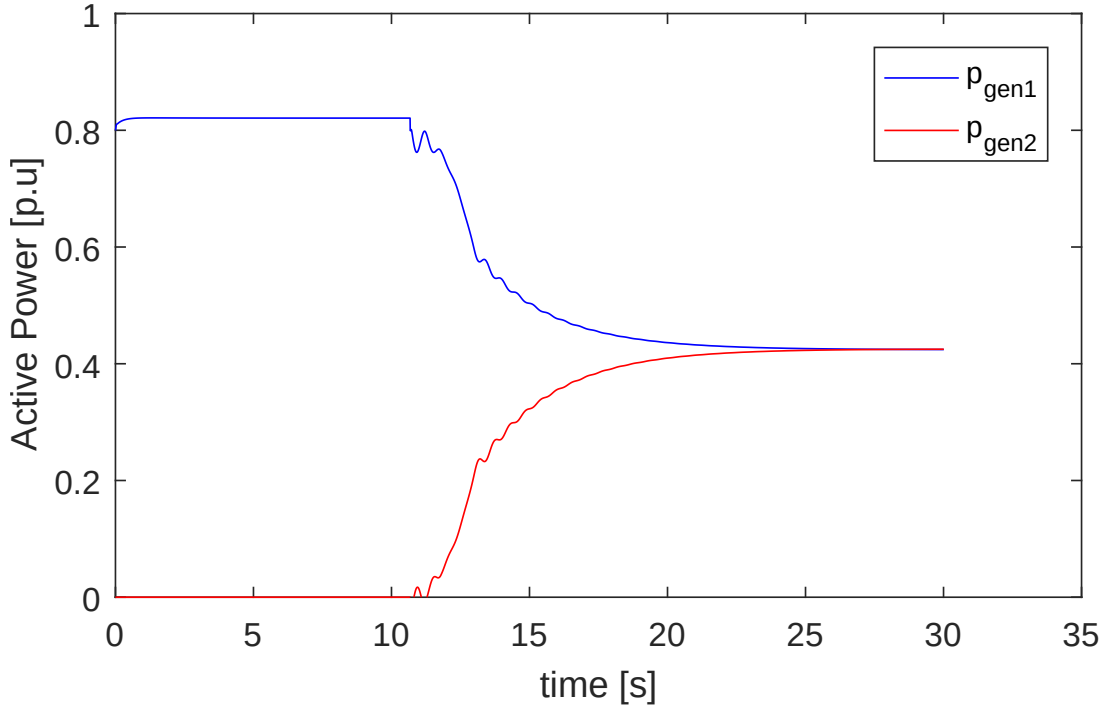

Figure 6.10: The active power of the two gensets being ramped after connecting genset 2 to the bus.

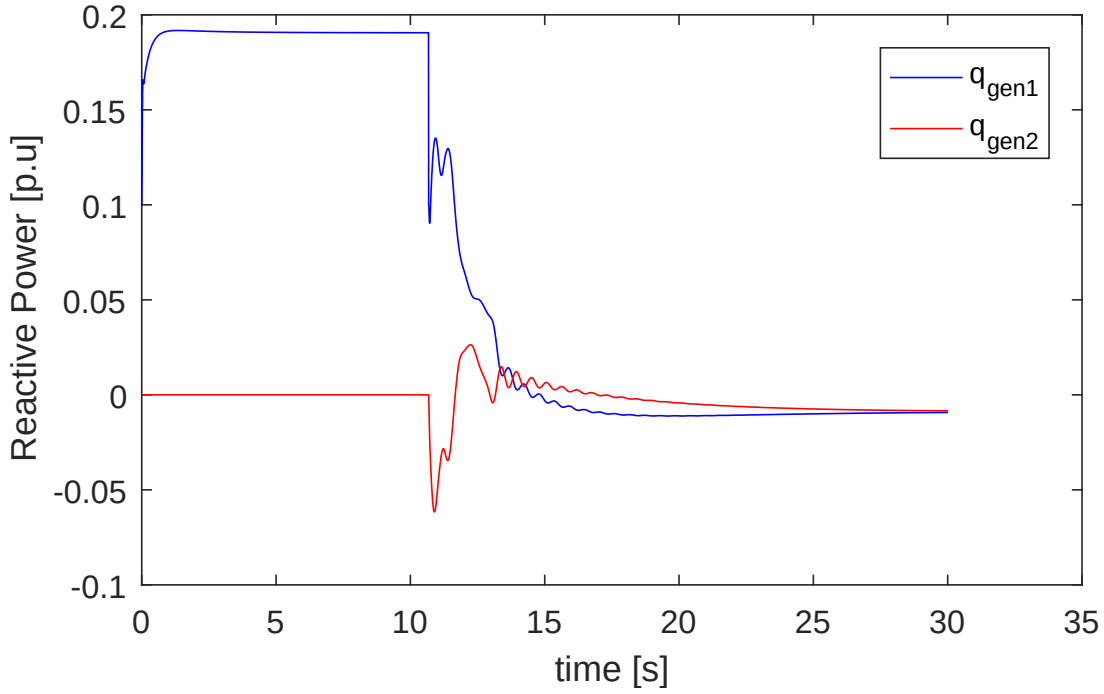

Figure 6.11: The reactive power of the two gensets being ramped after connecting genset 2 to the bus.

6.2.2 Discussion

For the first 4 seconds of the simulation, there are two gensets running where only one is connected to the bus, as seen in Figure 6.6. The timer τ_H builds up until it reaches $\tau_{Lim,H,2}$, which sets $\Omega = 1$ and initiates the synchronization process. The process begins with $\omega_{nl,2}$ and $V_{nl,2}$ being pushed towards ω_{bus} and V_{bus} respectively, as can be seen in Figures 6.7 and 6.8. This causes the frequency, ω_{gen2}, and the terminal voltage, V_{gen2}, of genset 2 to synchronize with the bus, as can be seen in 6.6 and 6.8.

When the synchronization is complete, the second genset is connected to the bus, this happens after approximate $10.5 seconds$. The no load frequency and voltage of genset 2 are now increased to match that of the other genset, the ramp up can be seen i Figure 6.9. The slow increase results in a load-up ramp of power, as can be seen in Figures 6.10. The active power $p_{gen,2}$ is loaded up by the steady increase of $\omega_{nl,2}$. There are some oscillations when loading up the active and reactive power of the gensets, these are due to oscillations in the gensets frequency after the connection. The active load sharing, seen in Figure 6.10, is functioning well, as p_{gen1} and p_{gen2} converge to $0.4[p.u.]$.

The reactive load sharing is not functioning as intended. Figure 6.11 show how the reactive power produced before connection is $q_{gen,1} = 0.19[p.u.]$ instead of $0.1[p.u.]$ as it is supposed to. After connection $V_{nl,2}$ is increased to ensure reactive load sharing between the gensets at $q_{gen} = 0.05[p.u.]$, however this is not the case. This behavior is most likely related to the spike in the bus voltage seen in Figure 6.8. Even though this is not the desired behavior, but it seems to have little influence on the overall system performance.

6.3 Varying load on the bus

Load changes on the bus causes the power produced by each connected generator to change. A simulation is executed where the load on the bus is ramped from $P_{bus,init} = 0.6[MW]$ to $P_{bus,final} = 0.8[MW]$. This increase is intended to cause a second genset to synchronize and connect to the bus.

Variable	Value	Unit
Gensets connected	1	[-]
Gen_{sb}	1	[MW]
$Pbus_{init}$	0.6	[MW]
$Qbus_{init}$	0.2	[MVA]
$\tau_{Lim,H,2}$	5	[s]
$p_{H,2}$	0.70	[p.u]

Table 6.3: Parameters for simulation of genset being connected.

6.3.1 Results

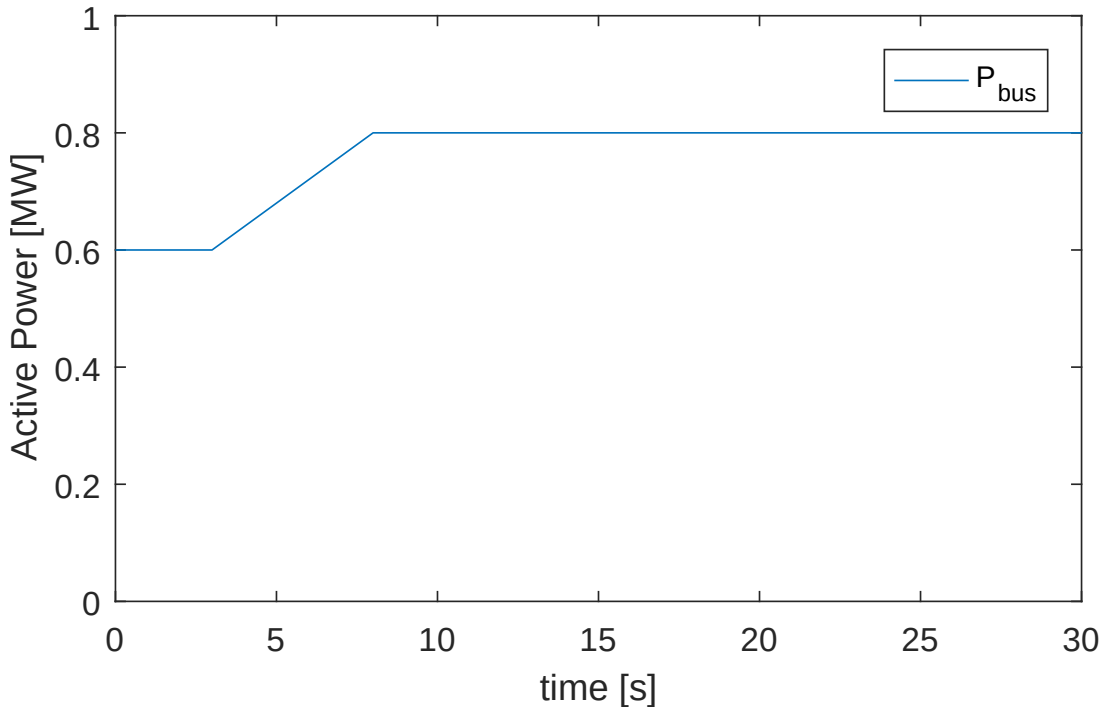

Figure 6.12: The active load on the bus being ramped.

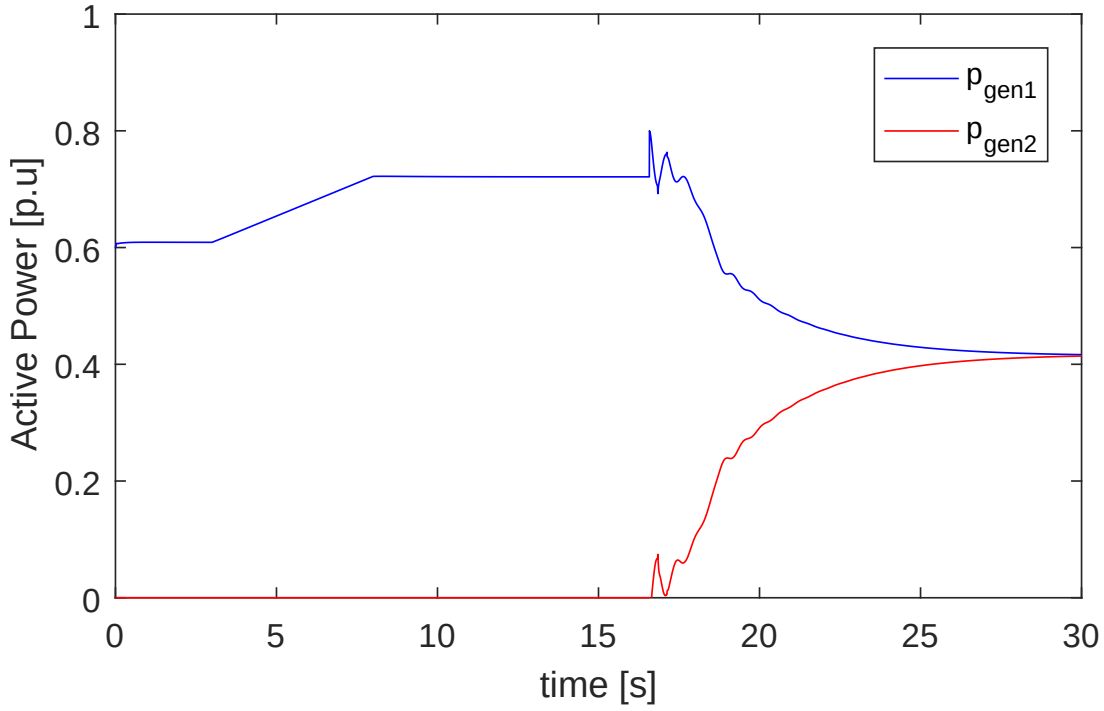

Figure 6.13: The active power of the two gensets in the varying load simulation.

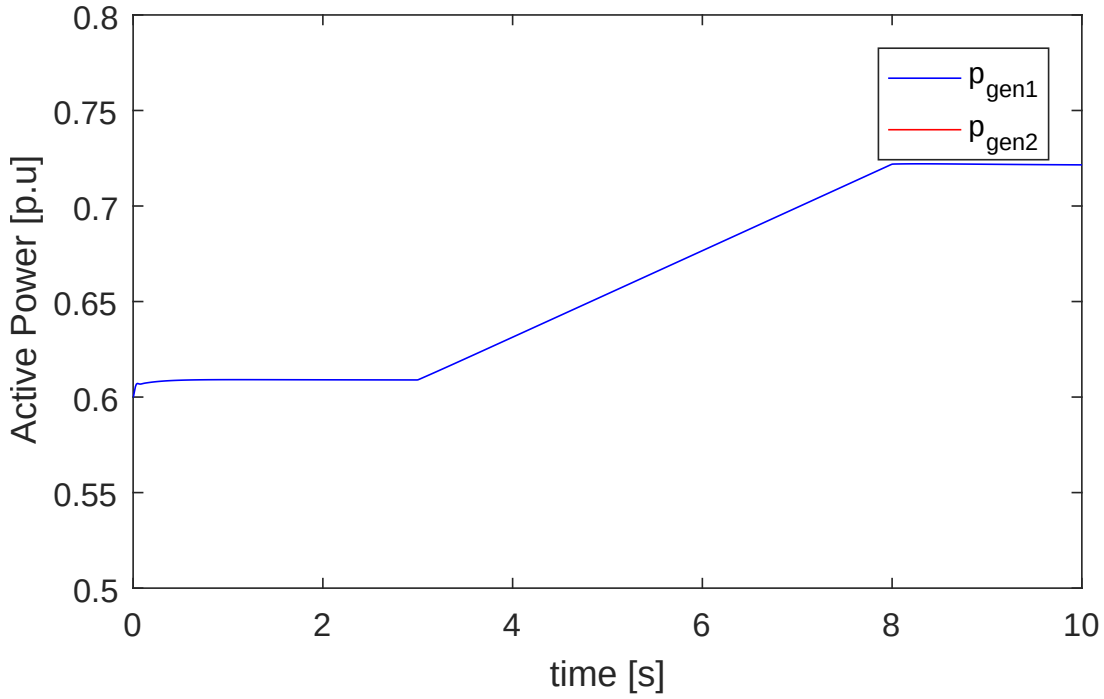

Figure 6.14: The active power of the active genset while the load is changed.

6.3.2 Discussion

With one genset connected with a base power of $1[MW]$, and an initial load on the bus of $P_{bus,init} = 0.6[MW]$, the genset supplies an active power of $p_{gen,1} = 0.6[p.u.]$ (Figures 6.12 and 6.13. When the load on the bus is steadily increased after $t = 3s$, the power produced by the genset also increases. However, the genset fails to deliver the power demanded by the bus, as $\dot{p}_{gen,1} < \dot{P}_{bus}$ during the ramp up to $P_{bus} = 0.8[MW]$. This causes the power delivered by the genset to be less than the actual load on the bus. After eight seconds when $P_{bus} = 0.8[MW]$, the power produced by the genset is only $P_{gen,1} = 0.72[p.u]$. This is unphysical, as more power is drawn from the system, than what is produced.

The power of genset 1 is adjusted when genset 2 is being connected. The jump map g sets $p_{gen,1}$ to its proper value. This causes the deviations of power produced to be adjusted whenever a jump is performed.

6.4 Conclusion

Ramping down and up both no load frequency and voltage in connect and disconnect operations are working as intended. The gensets are properly loaded-up when being connected and deloaded when being disconnected. However, there seem to be some issues with getting the correct powers delivered by the gensets when disconnecting. This is solved by jumping the active and reactive powers to their correct values. There is also an issue with ramping up the reactive load after connection of a new genset, and with reactive power generation in general.

The inability of the produced power to follow the power demanded by the bus greatly reduces the reliability of the simulator to perform fuel consumption and emission tests, as the power produced is inaccurate. The simulator resets the discrepancy after a new genset is being connected or disconnected, reducing the propagation of the inaccuracy.

The issues related to connecting and disconnecting gensets to and from the bus, and the processes related to these operations, does not seem to influence the overall performance of the simulator. The model is able to successfully connect and disconnect gensets with the synchronization and ramping that is necessary to do so.

Chapter 7

Efficiency of Marine Diesel Engines

7.1 Efficiency

Larger marine diesel engines are generally more efficient than smaller engines. Table 7.1 show a variety of medium- to high speed marine diesel engines, their rated power, mass and SFOC at optimal loading conditions. The trend shows how the medium speed engines capable of producing over 10MW have a lower SFOC than the high-speed marine engines with a lower rated power.

Engine type	Speed [RPM]	Power [MW]	SFOC [g/KWh]	Mass [Tonnes]
MAN V51/60DF	514	18	179	265
Wartsila 46F	600	19.2	170	233
MAN L48/60DF	514	10.8	175	148
Wartsila 38	600	11.6	180	110
MAN V32/44CR	750	10.8	175	79
Wartsila 31	750	9.7	170	89
MAN L32/44CR	750	4.8	172	50
Bergen B32:40L	750	4.5	184	46
MAN V28/33D STC	1000	5.4	188	38
Wartsila 26	1000	4	189	29
Bergen C25:33L	1000	3	185	25
Wartsila 20	1000	1.8	190	12

Table 7.1: Engine characteristics from (MAN, 2017), (Wartsila, 2017) and (Rolls-Royce, 2017)

Generator sets are generally less efficient than marine diesel engines, as a genset consists of a diesel engine and a generator. Table 7.2 show the parameters of two Perkins generator sets with noticably higher SFOC than the engines from Table 7.1.

Engine type	Speed [RPM]	Power [MW]	SFOC at 75%MCR [g/KWh]	Mass [Tonnes]
Perkins 4012-46TAG0A	1500	1	201	4
Perkins 2506C-E15TAG1	1500	0.4	212	1.6

Table 7.2: Genset characteristics ((Perkins, b) and (Perkins, a))

7.1.1 Specific Fuel Oil Consumption

The SFOC of an engine or a genset is highly dependent on the current percent of MCR the engine is running at, as introduced in Section 2.1. The ideal operating condition of a diesel engine is between $75-85$%MCR, as this is the range where the SFOC is at its minimum.

The illustrative SFOC curves for the two Perkins gensets are shown in Figure 7.1. The curves are based on data from (Perkins, b) and (Perkins, a), and the general profile of a SFOC-curve from (Ådnanes, 2003). The difference between the two gensets in SFOC at 75%MCR is 5.47%, this relationship is assumed to be constant for all percentages of MCR.

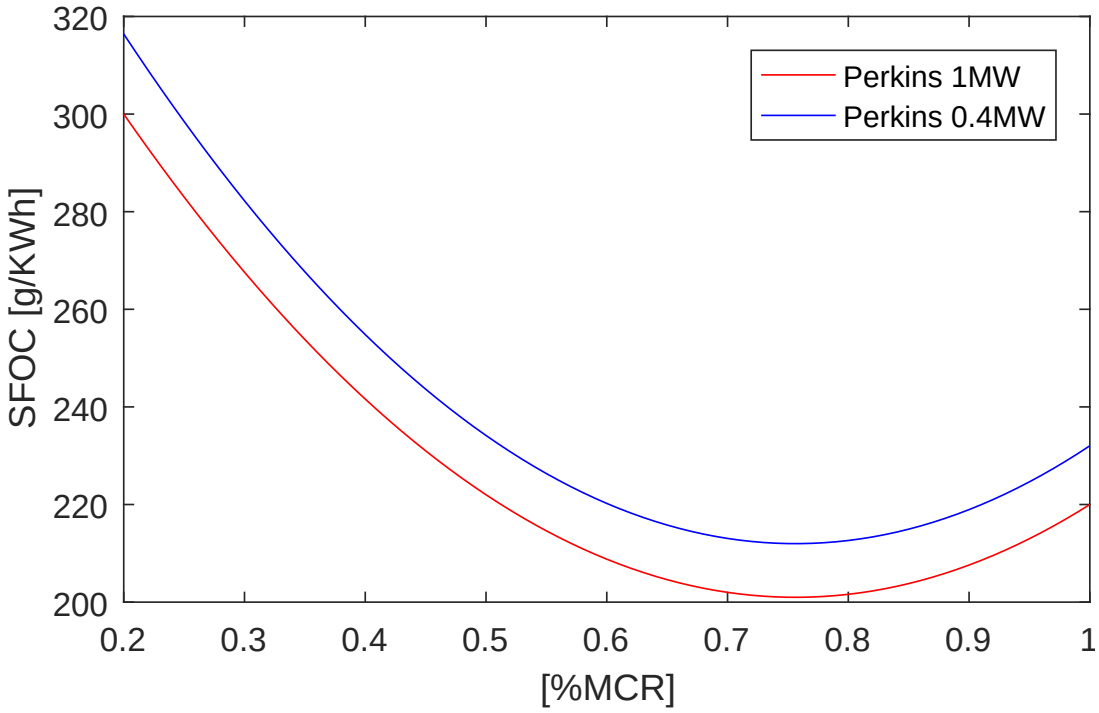

Figure 7.1: Illustrative SFOC-curves of the Perkins gensets from Table 7.2

7.2 Modeling Fuel Oil Consumption

SFOC-curves can be used to calculate the fuel consumed by using the following equation

$$F\dot{O}C = p_{gen}[MW] \cdot SFOC(p_{gen})[g/KWh] \tag{7.1}$$

$$= p_{gen}[MW] \cdot \frac{SFOC(p_{gen})}{3.6}[g/MWs], \tag{7.2}$$

where $F\dot{O}C$ is the Fuel Oil Consumption rate in $[g/s]$.

In order to calculate the fuel consumption rate of the entire power plant the equation above was adapted. It is for simplicity assumed that gensets that are disconnected from the bus does not consume any fuel. The equation becomes

$$F\dot{O}C = \sum_{i=1}^{N} p_{gen,i} \cdot c_i \frac{SFOC(p_{gen})}{3.6}, \tag{7.3}$$

where N is the number of gensets in the power plant and c is a boolean defining if a genset is connected to the bus.

Chapter 8

Case Study: Marine power plant with Varying Load

This section looks to study the fuel consumption of a marine power plant with a fixed capacity divided among few large engines and many smaller engines. The different configurations of engines are subjected to the same load variation on the bus, and the performance of each configuration is presented.

A marine power plant with a total power capacity of 4[MW] is chosen in the case study.

8.1 Load profile

Load profile describing the load on a marine power plant would ideally span over hours or days, describing different operations such as transit, DP, port etc.

Due to simulations taking roughly one day in real time to simulate one hour of a single genset, simulating a four genset or a thirty genset configuration for one hour would take four and thirty days, respectively. Therefore, the time span of the simulation is shortened and the load profile is simplified.

The load profile is chosen to test the marine power plant from a single genset connected to

the bus, to running every single one. The profile can be seen in Figure 8.1.

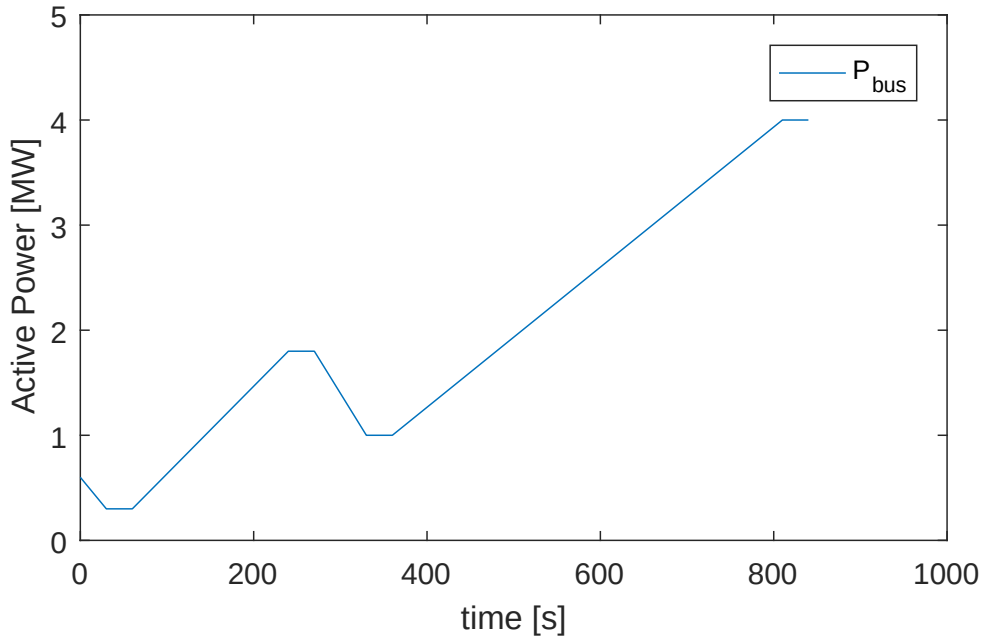

Figure 8.1: The load profile of the case study.

High frequency load variations from waves and wind are not included in the load profile. Ideally, wave loads would be included in the load profile, but due to the complications discussed in Section 6.3, the load profile is kept somewhat simple, in order to study the overall behaviour of the system.

8.2 Simulations

The same initial conditions and parameters are used for all simulations. The difference between the simulations are how many equally sized gensets make up the marine power plant.

Due to an irregularity during testing, the simulations are executed with no imaginary bus voltage component, i.e $\dot{\delta}_{bus} = 0$ and $\delta^{+}_{bus} = 0$.

The average power used to trigger the Start/Stop table is calculated based on P_{bus} instead of using p_{gen} as presented in Section 5.2. Due to the issues with calculating the power on each genset, discussed in Section 6.3, the following equation used to calculate average power becomes

$$p_{avg} = \frac{P_{bus}}{n \cdot S_{b,gen}} \tag{8.1}$$

where n is the number of connected gensets.

The start/stop configuration for the simulations are shown in Table 8.1.

	Stop gen		Start gen		Start gen	
n	p_L	$time_L$	p_H	$time_H$	p_{HH}	$time_{HH}$
1	-	-	60.0	10	98	1
2	27.5	10	72.5	10	98	1
3	38.3	10	80.0	10	98	1
4	43.7	10	83.8	10	98	1
5	47.0	10	86.0	10	98	1
6	49.2	10	87.5	10	98	1
7	50.7	10	88.6	10	98	1
8	51.9	10	89.4	10	98	1
9	52.8	10	90.0	10	98	1
10	53.5	10	90.5	10	98	1

Table 8.1: Simulation 1: Load dependent start table with two starting points for each number of gensets.

8.2.1 Simulation 1: 4 gensets

The first simulation is the 4[MW] marine power plant with four equally sized gensets with a rated power of 1[MW] each. The start/stop configuration can be seen in Table 8.1.

The genset used to calculate fuel consumption in simulation 1 is a Perkins 4012-46TAG0A from Table 7.2, with its SFOC consumption curve from Figure 7.1.

8.2.2 Simulation 2: 10 gensets

The second simulation is the 4[MW] marine power plant with ten equally sized gensets with a rated power of 0.4[MW] each. The start/stop configuration can be seen in Table 8.1.

The genset used to calculate fuel consumption in simulation 2 is a Perkins 2506C-E15TAG1 from Table 7.2, with its SFOC consumption curve from Figure 7.1.

8.3 Results

8.3.1 Simulation 1

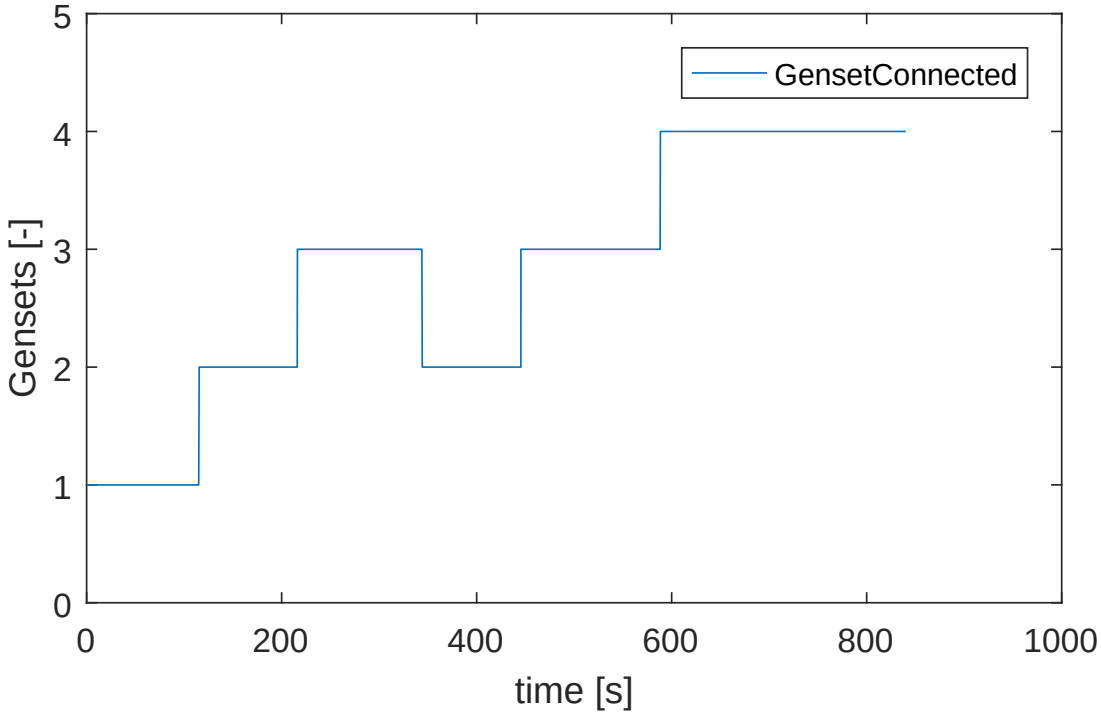

Figure 8.2: Simulation 1: The number of gensets connected to the bus.

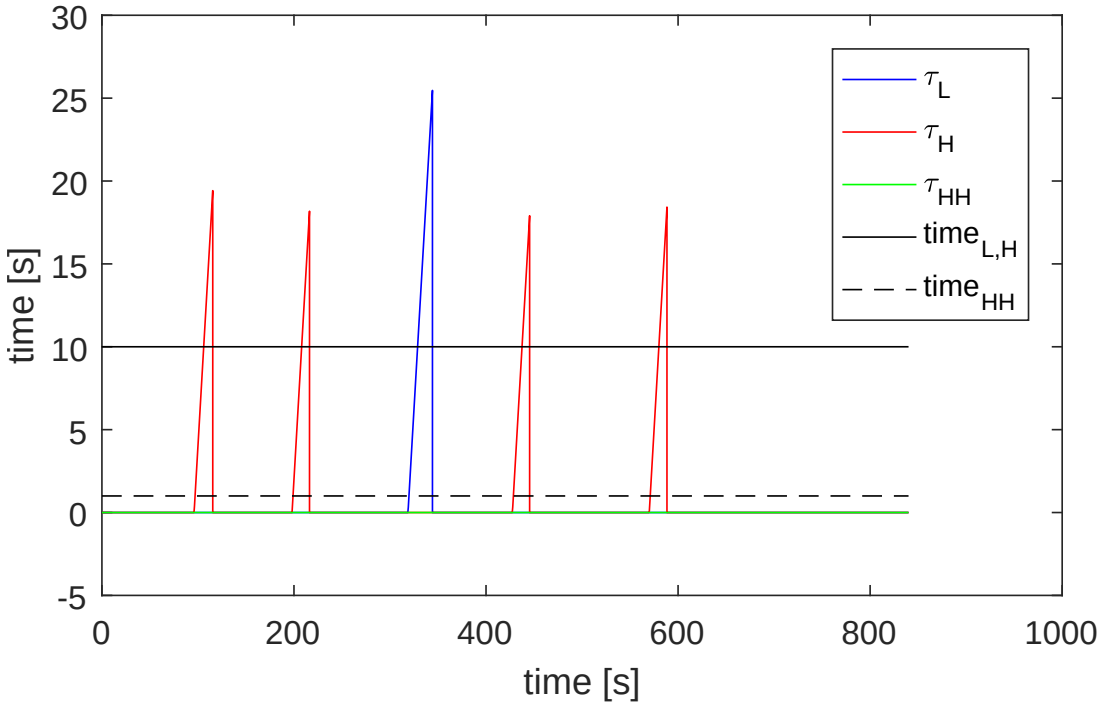

Figure 8.3: Simulation 1: The timers and time limits for connecting and disconnecting gensets.

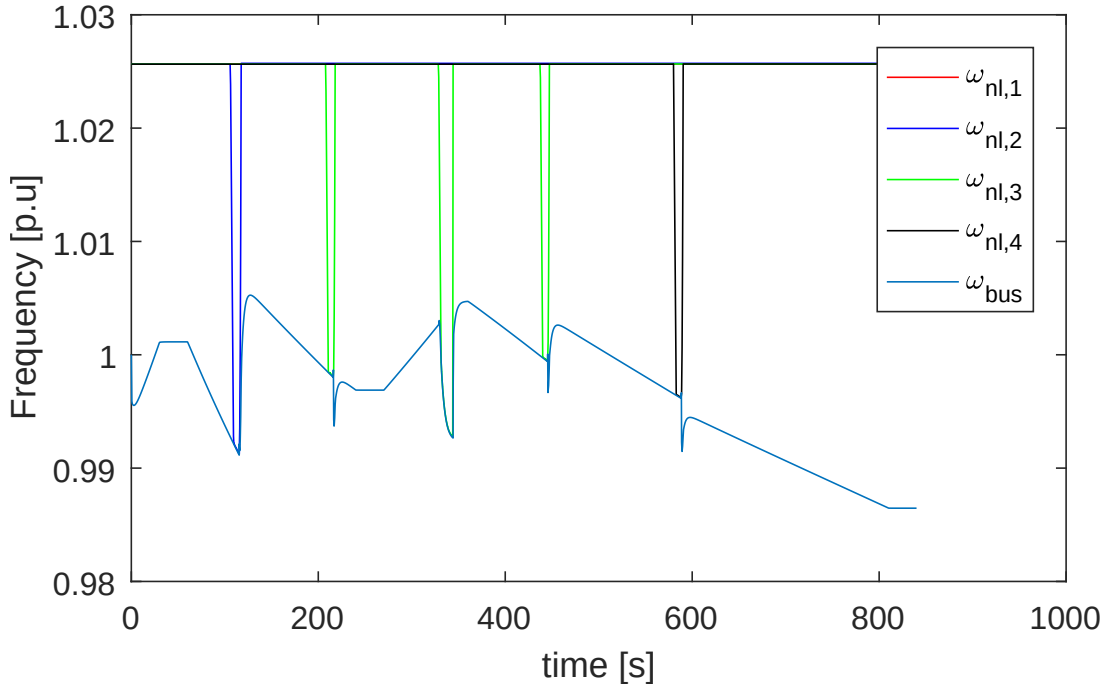

Figure 8.4: Simulation 1: The no-load frequency moving between a base value of 1.026 and the frequency of the bus for synchronization and load ramping.

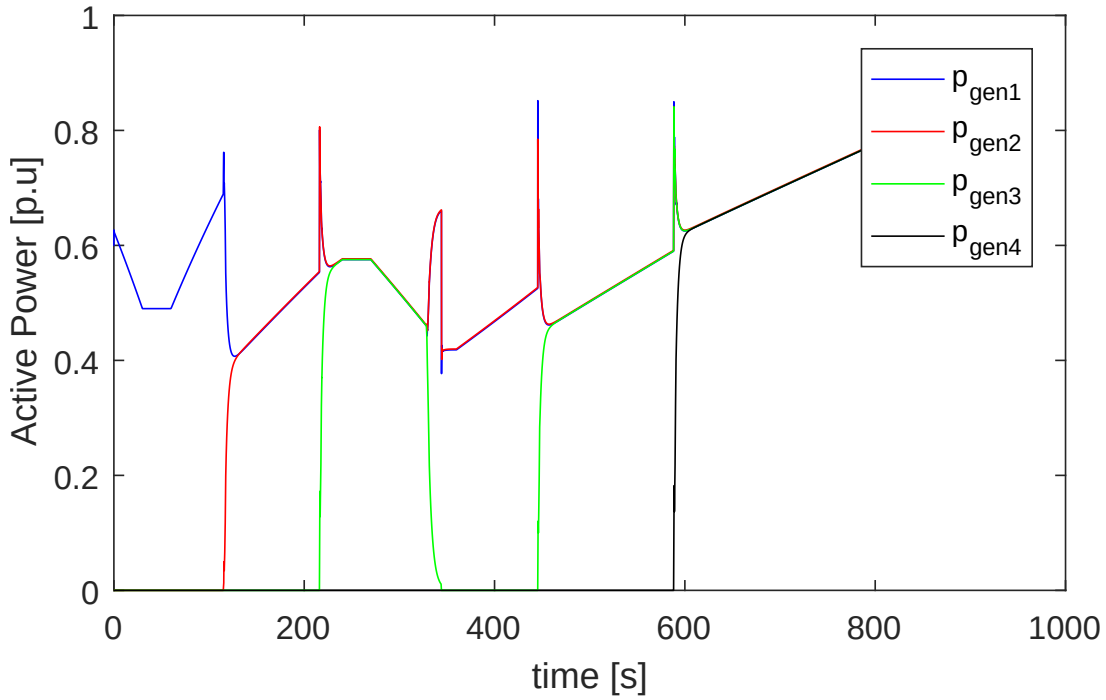

Figure 8.5: Simulation 1: The power produced by each genset.

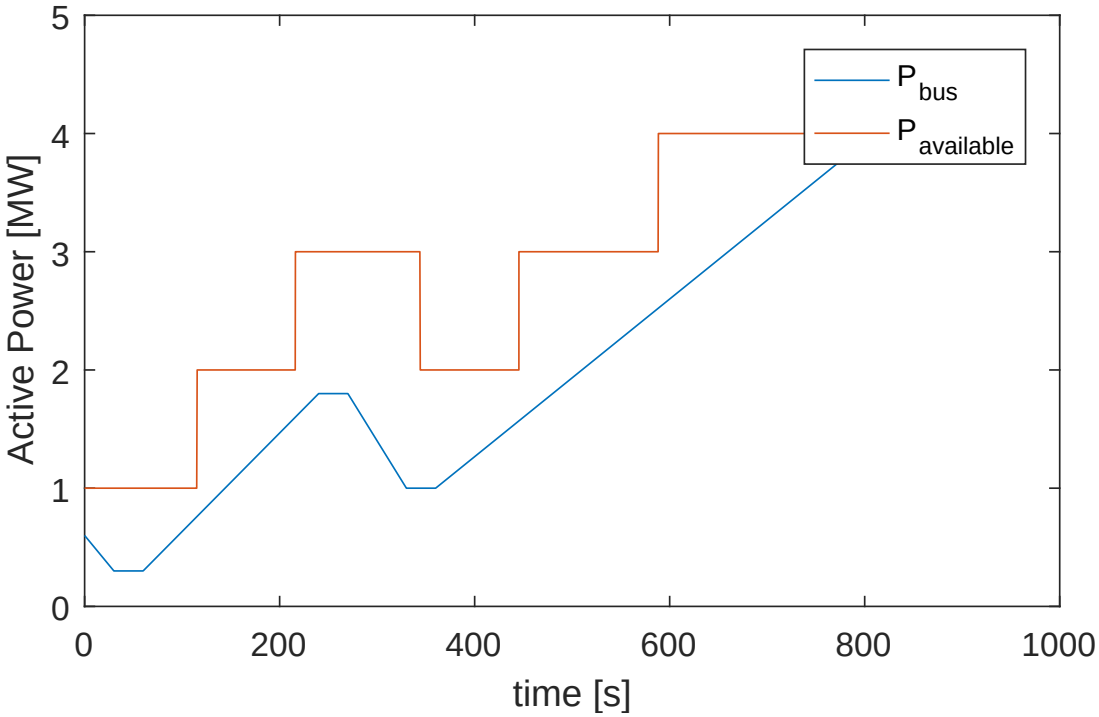

Figure 8.6: Simulation 1: Available power

8.3.2 Simulation 2

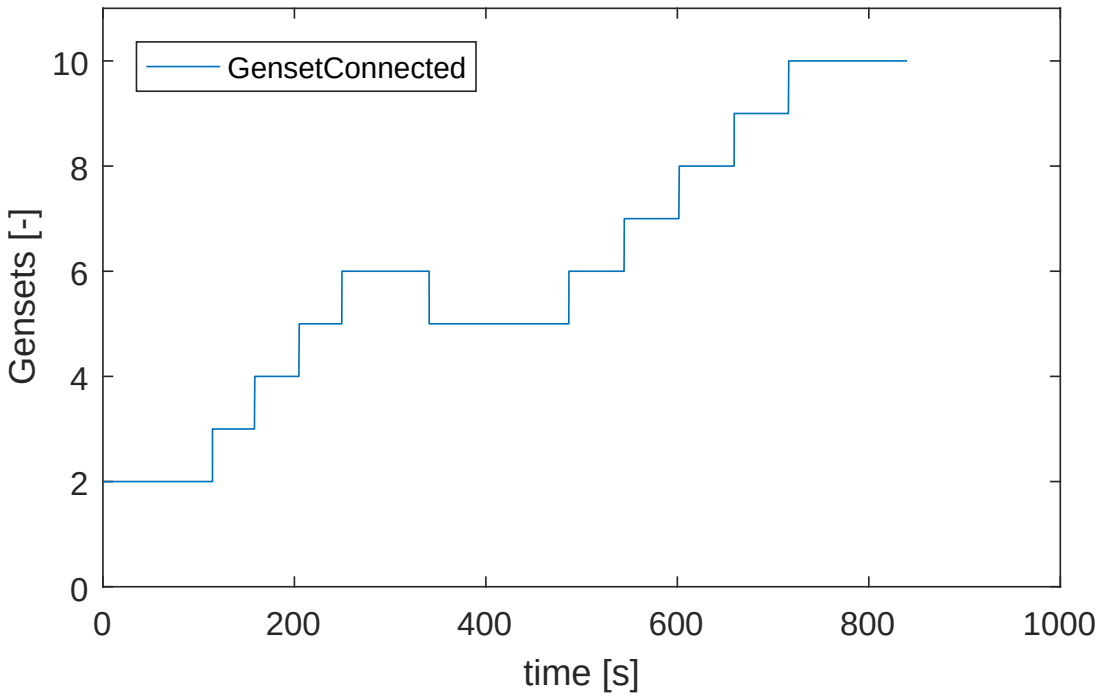

Figure 8.7: Simulation 2: The number of gensets connected to the bus.

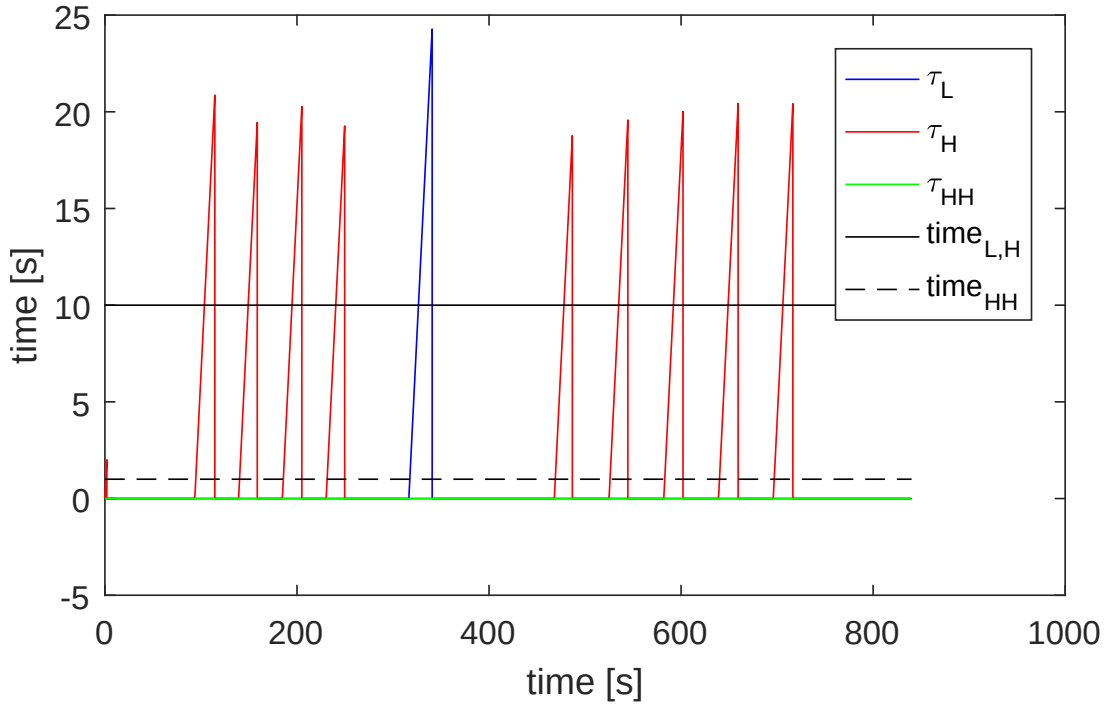

Figure 8.8: Simulation 2: The timers and time limits for connecting and disconnecting gensets.

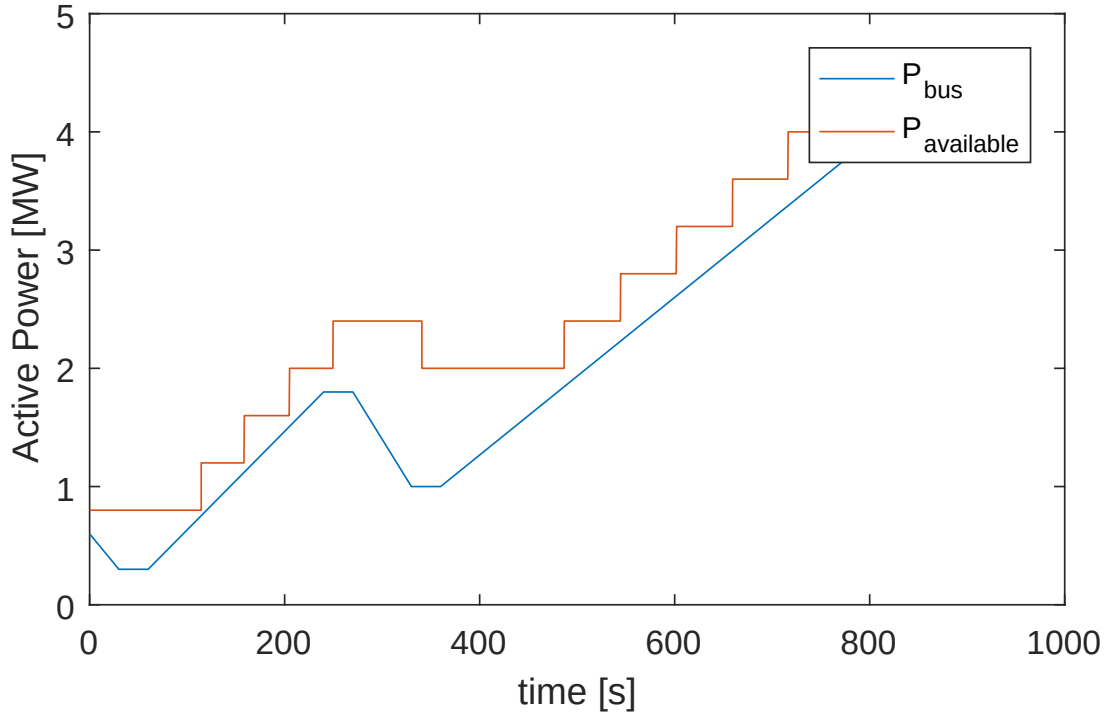

Figure 8.9: Simulation 2: Available power

8.3.3 Comparison and fuel consumption

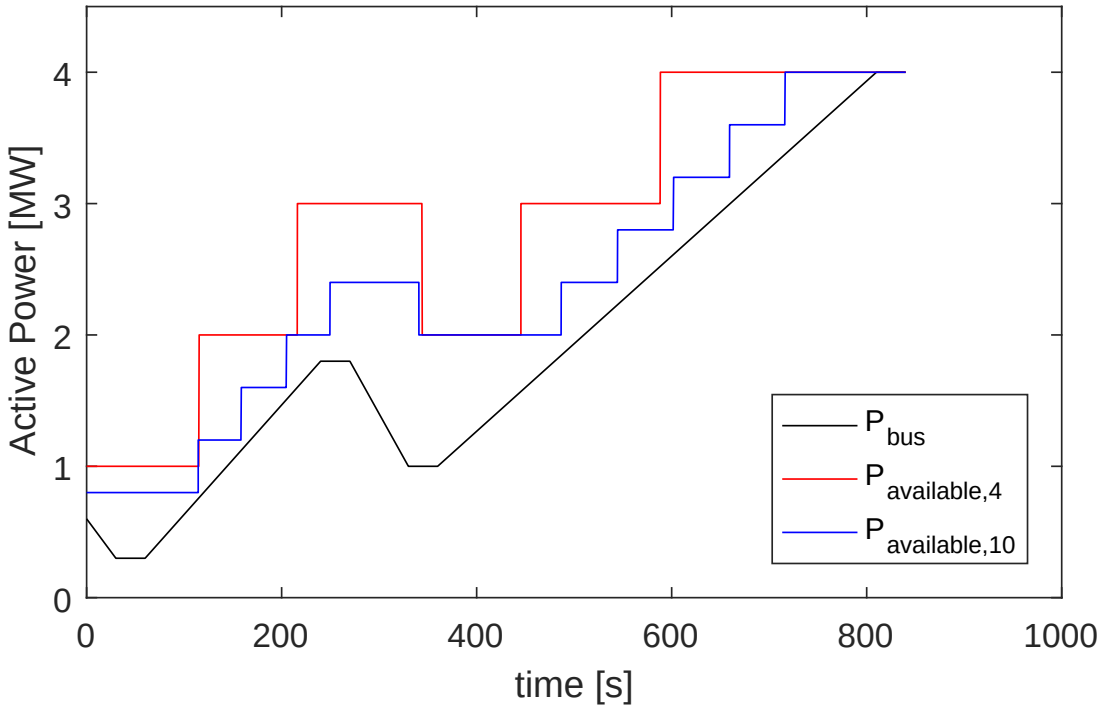

Figure 8.10: Simulation 1 and 2: The number of gensets connected to the bus.

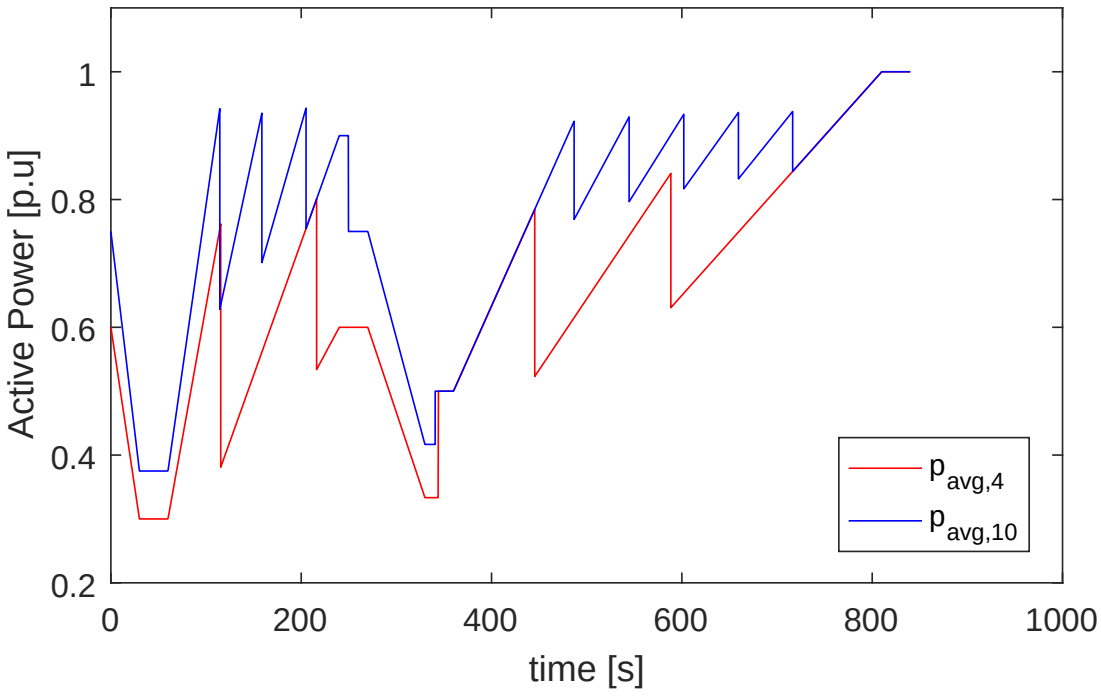

Figure 8.11: Simulation 1 and 2: The timers and time limits for connecting and disconnecting gensets.

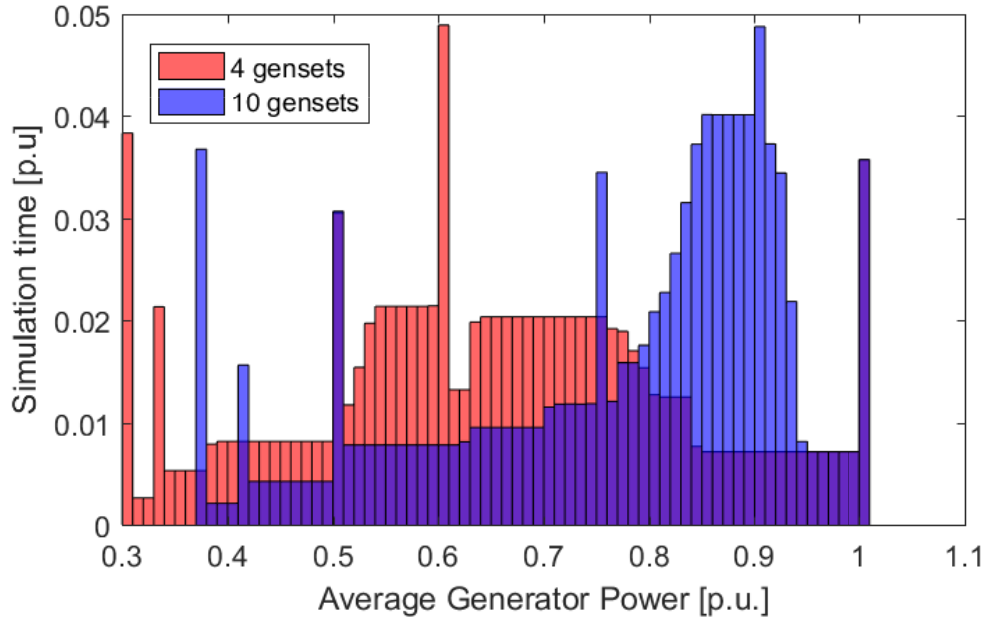

Figure 8.12: Simulation 1 and 2: The distribution of average generator power over the simulation.

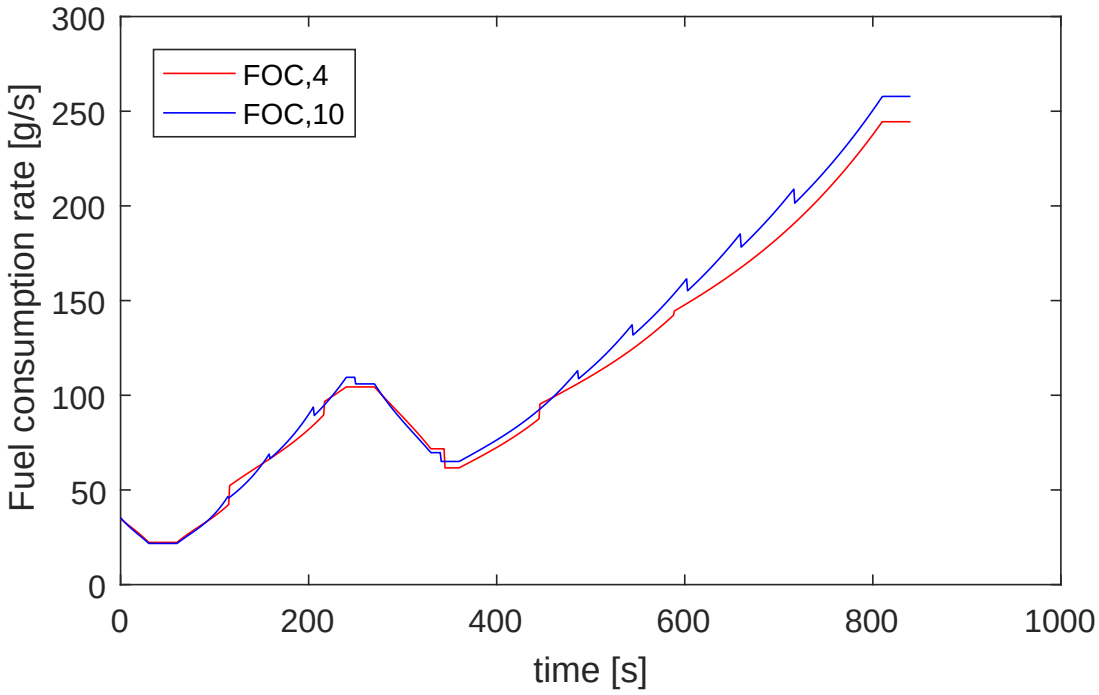

Figure 8.13: Simulation 1 and 2: The fuel consumption rate of the two simulated power plants.

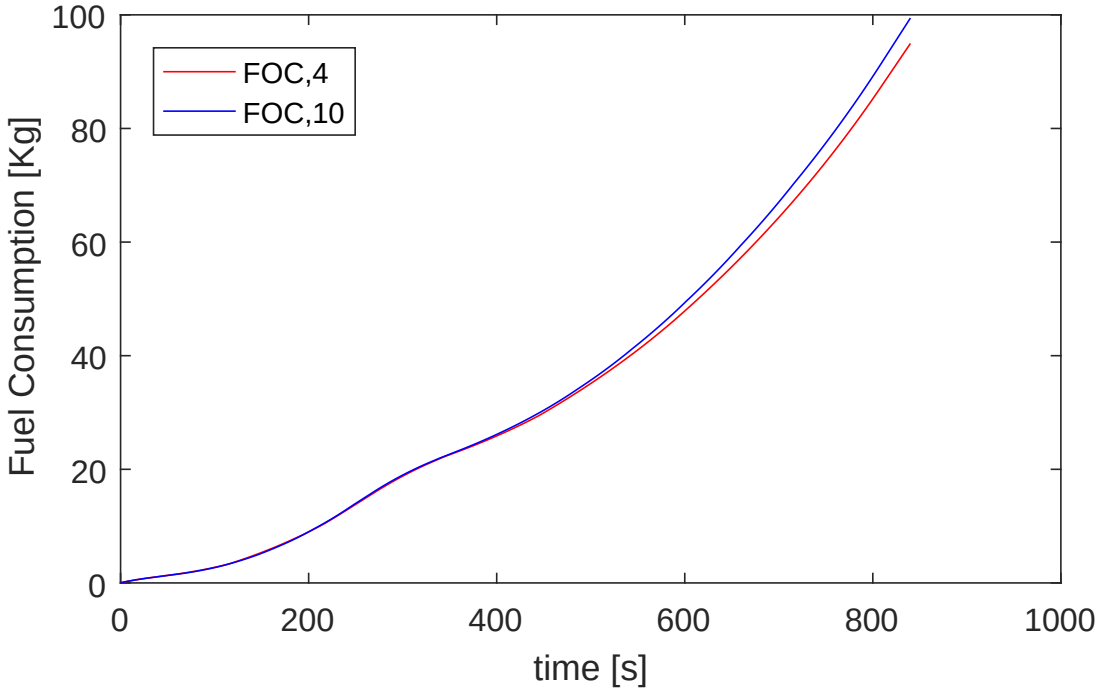

Figure 8.14: Simulation 1 and 2: The cumulative fuel consumed over the simulations.

8.4 Discussion

8.4.1 Simulation 1

The four-genset configuration properly connects and disconnects generator sets to the bus, as seen in Figure 8.2. Whenever the average power exceeds one of the limits p_L or p_H a timer is started, as seen in Figure 8.3. When the timers pass their respective limits $time_L$ and $time_H$ the necessary synchronization functions are initiated. As can be seen in Figure 8.3, the time it takes for a genset to synchronize and connect to the bus is roughly $8-10$ seconds while the deloading and disconnection of a genset takes about 15 seconds. The synchronization and deload times could be reduced, if desired, by increasing the PID gains of the governor during the processes of synchronization and de-loading.

The power produced delivered by each generator gives an inaccurate representation with regards to the power drawn by the bus. As seen in figure 8.5, the power delivered by each genset are significantly changed everytime the model performs a jump. The correct genset power values are calculated after each jump, and the issue lies with the continuous calculation of $\dot{p}_{gen}$, as discussed in section 6.3. The inaccuracy of $\dot{p}_{gen}$ become evident when the beginning of

the simulation is studied; with one genset connected and the load, P_{bus}, changing from 0.6 to 0.3[MW] (Figure 8.1), $p_{gen,1}$ should drop from 0.6 to 0.3[p.u.] but $p_{gen,1}$ does not drop below 0.5 [p.u], as can be seen in Figure 8.5.

Figure 8.4 show how the synchronization, ramp up load and deloading is achieved. The no-load frequency of the genset being connected or disconnected are reducing, as can be seen in the figure. The behaviour of the no-load frequency is discussed more in Sections 6.1 and 6.2.

By connecting a genset to the bus, the systems available power is increased by the gensets base power. Figure 8.6 show how the available power is incremented with a gensets base power, 1MW. The start/stop table ensures that the available power is always equal or larger than load on the bus, P_{bus}.

8.4.2 Simulation 2

The ten-genset configuration properly connects and disconnects gensets to the bus, as seen in Figure 8.2. Figure 8.8 show the behavior of the timers τ_L and τ_H. Similarly to the four-genset configuration, the synchronization process of a connecting genset lasts approximately $8-10$ seconds before the genset is connected to the bus. The single disconnection of a genset uses 14 seconds to disconnect.

Figure 8.9 show how the power plant increases its available power to supply the load on the bus, P_{bus}. With each genset being only 0.4MW, the increments of $P_{available}$ are smaller, allowing the power plant to adapt to smaller load changes on the bus. It should be mentioned that the available power between 100 and 200 seconds of simulations are a bit smaller than desired, i.e. the power plant is a bit slow in connecting new gensets. One is able to adjust the power available by tuning the Start/Stop table; in this case it would be desirable to decrease the power limits, $p_{H,n}$.

8.4.3 Comparison and fuel consumption

Figure 8.10 show available power from both simulations compared to the load on the bus. The marine power plant with ten engines is more able to adjust to a changing load P_{bus} than the four-engine configuration. This is due to the smaller size of the gensets in the second simulation reducing the increments of available power.

The ability to quickly adapt to the changing load allows the super-redundant power plant to operate within a specific range of average generator power, as can be seen in Figures 8.11 and 8.12. The first figure show how the ten-genset configuration is connecting gensets more frequent than the four-genset configuration, causing it to operate at a relatively steady average generator power between $0.8-0.9$[p.u], as illustrated in the histogram in Figure 8.12. The simulation with four gensets gives more spread in average generator power with values mainly ranging between $0.5-0.8$[p.u.].

The SFOC-curves from Figure 7.1 have an ideal operating point of 75%MCR. This optimal operating point is not matched by that of the ten-genset simulation, which mainly ranges between $80-90$%MCR. Ideally the start/stop table should be tuned in order to operate the gensets at optimal %MCR with respect to SFOC, this is however not the case for the super-redundant simulation. If the average generator power of the ten-genset simulation (Figure 8.12) were centered around 75% insted of 87%MCR, there would be a 4% reduction in SFOC during most of the super-redundant simulation.

The fuel consumption rate and the cumulative fuel consumption of the two simulations is shown in Figures 8.13 and 8.14, respectively. While the power plants are operating at loads below 25% of total capacity (0-200 seconds) the two configurations are consuming approximately the same amount of fuel, with only a 0.1% difference. Between 200 and 500 seconds, the ten-genset power plant consumes 2.2% more fuel than the four-genset configuration. After 500 seconds, the fuel consumption rate of the ten-genset configuration is 6.5% higher than that of the four-genset power plant. This results in a total of 4.7% fuel consumed by the super-redundant configuration. Taking a properly tuned start/stop table into consideration, the super-redundant power plant could potentially outperform a conventional marine power plant at both low and medium loads.

8.5 Conclusion

The ten-genset configuration is able to adapt to smaller changes in the changing load on the bus, however the SFOC of a single genset in the super-redundant marine power plant is higher due to smaller engines generally being less efficient.

A conventional four-genset marine power plant configuration outperforms a ten-genset configuration at higher loads, while at lower loads the difference is negligeble. Considering a properly tuned start/stop table, the ten-genset marine power plant could potentially reduce fuel consumption with up to 4% compared to the case study, this would suggest that a super-redundant marine power plant is more efficient than conventional configurations, especially while operating below 50% of the power plants total power capacity.

Chapter 9

Maintenance and Redundancy

The use of super-redundant marine power plant with up to 30 gensets comes with advantages and disadvantages when compared to a more conventional diesel electric power plant configuration with only four engines.

9.1 Maintenance

More engines running generally results in an increase of maintenance. With the assumption that the mean time to failure (MTTF) of a genset is independent of its rated power, more running gensets gives more failures in total. More failures in generators increases the demand of maintenance and repairs.

There are potential savings in maintenance for vessels with super-redundant power plants that often visit the same port. Due to the gensets relatively small size, a faulty genset could be swapped with a functioning one at port, reducing costly maintenance and downtime at sea. There would be the need for a module-based system, where gensets could easily be removed and new one installed without causing the vessel to stay at port for longer than intended.

9.2 Redundancy

The impact of a genset failure would have a smaller on a super-redundant marine power plant than a regular power plant with fewer gensets. A power plant with only four gensets would lose 25% of its total power in the case of a single failure, while a super-redundant plant with 30 gensets would only lose 3.3% (Figure 9.1). This allows a super-redundant marine power plant to continue operations after a genset failure, where a regular power plant possibly would have to abort due to a shortage in power production.

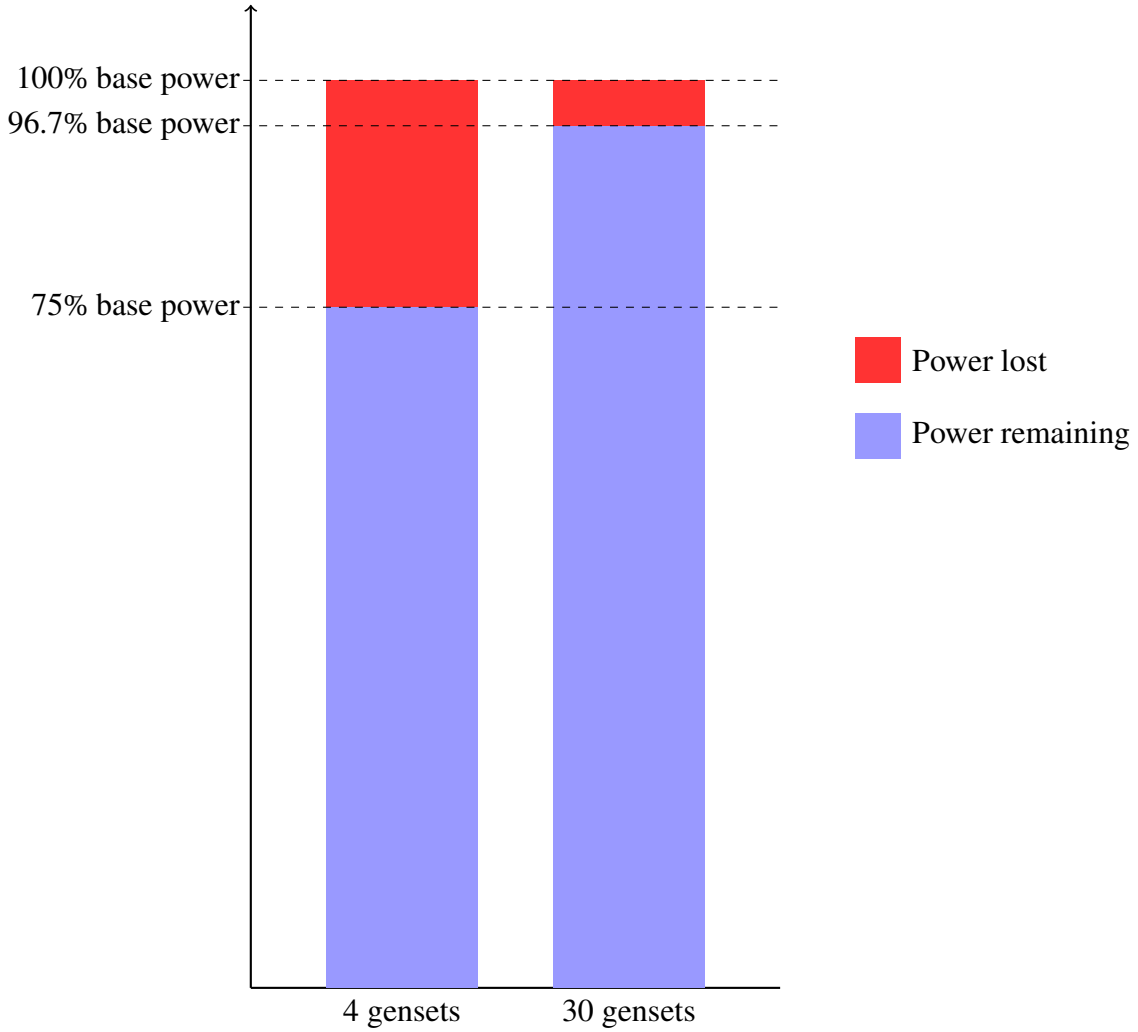

Figure 9.1: The effect of a single genset failure on the power plants total power capacity. Comparing a 4 genset configuration with a super-redundant plant with 30 gensets.

Chapter 10

Conclusion and Recommendation for Further Work

The hybrid dynamical model is able to successfully connect and disconnect gensets with the synchronization and ramping that is necessary to do so, and provide equal load sharing among the active gensets. By using the hybrid dynamical framework for the marine power plant model, both continuous and discrete behaviors could be included.

The case study show how a conventional four-genset marine power plant configuration outperforms a ten-genset configuration at higher loads, while at lower loads the difference is negligible. Considering a properly tuned start/stop table, the ten-genset marine power plant could potentially reduce fuel consumption with up to 4% compared to the case study, this would suggest that a super-redundant marine power plant is more efficient than conventional configurations, especially while operating below 50% of the power plants total power capacity.

With potential savings on fuel consumption, emissions, maintenance, and an increased redundancy, a super-redundant marine power plant could become commercially viable and contribute to reduce emissions from maritime industry.

10.1 Recommendation for Further Work

- Implement a better model for calculating the power produced in each genset, p_{gen}.
- Enable the connection/disconnection of more than one genset at a time.
- Properly stop the gensets that are not connected to the bus.
- Calculate emissions of a configuration by using emission lookup tables.
- Study sooting and emissions related to rapid start/stop operations.

Bibliography

Bø, T. I. (2012). Dynamic model predictive control for load sharing in electric power plants for ships. Master's thesis, NTNU.

Bird, J. (2007). *Electrical Circuit Theory and Technology*. Electrical circuit theory and technology series. Newnes.

Ådnanes, A. K. (2003). Technical report, ABB AS Marine.

Eleftherios K. Dedes, Dominic A. Hudson, S. R. T. (2012). Assessing the potential of hybrid energy technology to reduce exhaust emissions from global shipping. *Energy Policy*, 40:204–218.

Goebel, R. (2012). *Hybrid Dynamical Systems: Modeling, Stability, and Robustness*. Princeton University Press.

I. Jadric, D. Borojevic, M. J. (2002). Modeling and control of a synchronous generator with an active dc load. *IEEE*, pages 303 – 311.

IMO (2009). Second imo green house emission study. international maritime organisation.

IMO (2012). International shipping facts and figures – information resources on trade, safety, security, environment.

IMO (2014). Third imo green house emission study. international maritime organisation.

Ingebrigtsen Bø, T. (2016). *Scenario- and Optimization-Based Control of Marine Electric Power Systems*. PhD thesis, NTNU.

Issam Baghdadi, Olivier Briat, J.-Y. D. (2016). Lithium battery aging model based on dakin's degradation approach. *Journal of Power Sources 325 273-285*.

J.N. Hu, J.J. Hu, H. L. (2014). State-of-charge estimation for battery management system using optimized support vector machine for regression. *Journal of Power Sources 269*, pages 682–693.

Kong Soon Ng, Chin-Sien Moo, Y.-P. C. (2009). Enhanced coulomb counting method for estimating state-of-charge and state-of-health of lithium-ion batteries. *Applied Energy*, (86):1506–1511.

Krause, P., Wasynczuk, O., Sudhoff, S., and Society, I. P. E. (2002). *Analysis of electric machinery and drive systems*. IEEE Press series on power engineering. IEEE Press.

MAN (2017). Man marine engines and systems.

Olivier Tremblay, Louis-A. Dessaint, A.-I. D. (2007). A generic battery model for the dynamic simulation of hybrid electric vehicles. *IEEE Vehicle Power and Propulsion Conference*, pages 284–289.

Perkins. Perkins 2506c-e15tag1.

Perkins. Perkins 4012-46tag.

R. K. Mallick, R. K. P. (2011). Fault analysis of voltage-source converter based multi-terminal hvdc transmission links. *IEEE ICEAS*, 5:1–7.

Rolls-Royce (2017). Rolls royce medium speed diesel engines.

Sanfelice, R. (2016). Hybrid equations toolbox v2.03.

Skjetne, R. (2016). Work note: Load-dependent start and stop of gensets modeled as a hybrid dynamical system.

T. Waldmann, M. Wilka, M. K. (2014). Temperature dependent ageing mechanisms in lithium-ion batteries: a postmortem study. *J. Power Sources 262 129-135.*

Torstein I. Bø, Andreas R. Dahl, T. A. J. (2015). Marine vessel and power plant system simulator. *IEEE Access*, pages 2065–2079.

Umer Amir Khan, Jong-Geon Lee, F. A. (2015). A novel model of hvdc hybrid-type superconducting circuit breaker and its performance analysis for limiting and breaking dc fault currents. *IEEE TRANSACTIONS ON APPLIED SUPERCONDUCTIVITY*, 5.

Wartsila (2017). Wartsila diesel engines.

Woo-Young Choi, C.-G. L. (2011). Photovoltaic panel integrated power conditioning system using a high efficiency step-up dc–dc converter. *Elsevier Renewable Energy*, pages 227–234.

Woodward. Governing fundamentals and power management. Reference Manual 26260.

Yao He, XingTao Liu, C. Z. (2013). A new model for state-of-charge (soc) estimation for high-power li-ion batteries. *Applied Energy*, (101):808–814.

Yinjiao Xing a, Wei He, M. P. (2014). State of charge estimation of lithium-ion batteries using the open-circuit voltage at various ambient temperatures. *Applied Energy*, (113):106–115.

Yinquan Hu, Xiaobing Wu, J. T. (2015). Research of power battery management system in electric vehicle. *International Journal of Multimedia and Ubiquitous Engineering*, pages 187–194.

Zhang, X. Y. H. L. J. (2011). *Lithium-Ion Batteries: Advanced Materials and Technologies*. CRC Press.